Dark matter as the trigger of flavor changing neutral current decays of the top quark

Adil Jueid[1,*] and Shinya Kanemura[2,†]

[1]*Particle Theory and Cosmology Group, Center for Theoretical Physics of the Universe, Institute for Basic Science (IBS), Daejeon, 34126, Republic of Korea*
[2]*Department of Physics, Osaka University, Toyonaka, Osaka 560-0043, Japan*

(Received 16 April 2024; accepted 10 October 2024; published 12 November 2024)

We suggest a simplified model that simultaneously addresses the dark matter problem and gives rise to top-quark flavor changing neutral current (FCNC) interactions at the one-loop order. The model consists of two extra $SU(2)_L$ gauge singlets: a colored mediator of spin zero (S) and a right-handed fermion (χ); both are odd under an *ad hoc* Z_2 symmetry. The right-handed fermion plays the role of the dark matter candidate. In this model, the presence of the two dark sector particles generates one-loop induced FCNC decays of the top quark into light quarks and bosons such as the gluon, the photon, the Z boson, or the Higgs boson. As a case study, we analyze the top-quark FCNC decays into light quarks (u or c) and Z or Higgs bosons. We then study the reliable solutions to the dark matter problem by estimating the regions in the parameter space that are consistent with the *Planck* measurement of the dark matter relic density. We also revisit the bounds from the searches of dark matter in events with at least one high-p_T jet and large missing transverse energy at the Large Hadron Collider (LHC). We then define four benchmark points that are consistent with the existing constraints from collider experiments and cosmology. We finally estimate, for these benchmark scenarios, the rates of a broad range of channels that can be used to probe the connection between the top FCNC transitions and dark matter, both at the HL-LHC and at a future 100 TeV collider.

DOI: 10.1103/PhysRevD.110.095009

I. INTRODUCTION

The Standard Model (SM) of elementary particles predicts that tree-level flavor changing neutral current (FCNC) transition rates are exactly zero, including those of the top quark. The reason for this is that the biunitary transformations that diagonalize the fermion mass matrices lead to diagonal couplings of the Higgs and the Z bosons to fermions. At the one-loop order, the rates of, e.g., top-quark FCNC decays are very suppressed thanks to the Glashow-Iliopoulos-Maiani (GIM) mechanism [1]. As a consequence of the GIM mechanism, the suppression of the top-quark FCNC rates at the one-loop order is due to the unitarity of the Cabibbo-Kobayashi-Maskawa (CKM) matrix and the smallness of the mass splittings between the different quarks running in the loop. The calculation of the top-quark FCNC decay rates in the SM was performed nearly 33 years ago by the authors of Ref. [2]. It is found that the branching ratios of $t \to cX$ and $t \to uX$ are generally very small, ranging from 10^{-17} to 10^{-12}. Such small rates imply that any observation of the top-quark FCNC phenomena at the LHC is a clear sign of new physics beyond the SM (BSM). Several BSM models may give rise to sizeable rates for the top-quark FCNC decays [3–31].[1] Searches of top-quark FCNC interactions have been carried out at the LHC by the ATLAS [32–42] and the CMS collaborations [43–47]. It has been found that bounds on the top-quark FCNC branching ratios have been improved by about an order of magnitude. This achievement is due to two important factors: (*i*) the increase of both the center-of-mass energy of the pp collisions at the LHC and of the accumulated luminosity, and (*ii*) the improvements on the analysis techniques used to perform the signal-to-background optimization—i.e., going from simple cut-based methods to novel machine learning techniques. It is expected that the HL-LHC with 3000 fb^{-1} of integrated luminosity would enable more stringent bounds on the top-quark FCNC decays, which would therefore put stronger constraints on various BSM scenarios.

*Contact author: adiljueid@ibs.re.kr
†Contact author: kanemu@het.phys.sci.osaka-u.ac.jp

[1]In Table I, we give a summary of the branching ratios of the top-quark FCNC decays in the SM and some of the well-known BSM extensions.

TABLE I. Summary of the branching ratios for top-quark FCNC decays in the SM along with the highest predicted values in several well-known BSM extensions. The results are taken from the 2013 Top Working Group Report [74].

Process	SM	2HDM (FC)	2HDM (FV)	MSSM	RPV-MSSM	RS
$\mathrm{BR}(t \to Zc)$	1×10^{-14}	$<10^{-10}$	$<10^{-6}$	$<10^{-7}$	$<10^{-6}$	$<10^{-5}$
$\mathrm{BR}(t \to Zu)$	7×10^{-17}	⋯	⋯	$<10^{-7}$	$<10^{-6}$	⋯
$\mathrm{BR}(t \to gc)$	5×10^{-12}	$<10^{-8}$	$<10^{-4}$	$<10^{-7}$	$<10^{-6}$	$<10^{-10}$
$\mathrm{BR}(t \to gu)$	4×10^{-14}	⋯	⋯	$<10^{-7}$	$<10^{-6}$	⋯
$\mathrm{BR}(t \to \gamma c)$	5×10^{-14}	$<10^{-9}$	$<10^{-7}$	$<10^{-8}$	$<10^{-9}$	$<10^{-9}$
$\mathrm{BR}(t \to \gamma u)$	4×10^{-16}	⋯	⋯	$<10^{-8}$	$<10^{-9}$	⋯
$\mathrm{BR}(t \to Hc)$	3×10^{-15}	$<10^{-5}$	$<2 \times 10^{-3}$	$<10^{-5}$	$<10^{-9}$	$<10^{-4}$
$\mathrm{BR}(t \to Hu)$	2×10^{-17}	⋯	$<6 \times 10^{-6}$	$<10^{-5}$	$<10^{-9}$	⋯

In this study, we consider the possibility that dark matter (DM) and top-quark FCNC transitions are connected via new particles that are odd under an *ad hoc* Z_2 symmetry. In this category of models, both the production of DM at hadron colliders and its self-annihilation in the Universe are mediated by colored mediators in t-channel diagrams. The DM phenomenology at colliders is minimally realized by extending the SM by one mediator (Y) that transforms as a triplet under $SU(3)_c$ and a neutral particle (X) under $U(1)_Y$. The mediators can transform, however, either as singlets or as doublets under $SU(2)_L$, while the DM candidate must always transform as a singlet. Assuming that the colored mediator is a singlet under $SU(2)_L$, there are 12 possible categories for these models, depending on the underlying assumptions on the spin of the mediators and of the DM candidate. The phenomenology of this class of models has been extensively studied in the literature [48–61]. In the most minimal realizations of these scenarios, the main assumption that has usually been used is that each mediator couples *solely* to one quark generation. This assumption is motivated by the requirement to avoid one-loop induced FCNC transitions. Here, we assume, however, that the colored mediator(s) can couple simultaneously to all the quark generations with *generally* different coupling parameters. We consider a minimal extension that contains one colored scalar that possesses the same quantum numbers as a right-handed up-type quark and a Majorana fermion; both are singlets under $SU(2)_L$. By taking into account this assumption, this model will lead to nonzero rates for top-quark FCNC transitions at the one-loop order. By analyzing the top-quark FCNC decays into qZ and qH within this model and studying the possible constraints from collider experiments and cosmology, we find interesting scenarios that may be amenable to discovery, both at the HL-LHC and at a future 100 TeV collider.

The rest of this manuscript is organized as follows: In Sec. II, we present the model and its particle content. We discuss in detail the branching ratios for top-quark FCNC decays into qZ and qH in Sec. III. Section IV is devoted to an analysis of the DM relic density within this model. The impact of LHC constraints from searches of DM in events with multijets plus missing energy on our model is discussed in Sec. V. We present four benchmark scenarios and discuss their characteristics in Sec. VI. We draw our conclusions in Sec. VII.

II. THEORETICAL FRAMEWORK

In this work, we consider a minimal simplified model with a t-channel scalar mediator (S) that carries a color charge and a right-handed fermion (χ) that plays the role of the DM candidate. In this framework, the DM particle interacts primarily with SM quarks through a Yukawa-type interaction. In this study, we consider one possible scenario where the scalar mediator couples to right-handed up-type quarks.[2] In this framework, the new states transform as

$$S:(\mathbf{3},\mathbf{1})_{+2/3}, \qquad \chi:(\mathbf{1},\mathbf{1})_0, \tag{2.1}$$

where the numbers refer to their representations under $SU(3)_c \otimes SU(2)_L \otimes U(1)_Y$. On the other hand, both the scalar mediator and the DM candidate are odd under Z_2 symmetry, while all the SM particles are even. To ensure that the DM particle is stable, we also require that $M_\chi \leqslant M_S$. The most general Lagrangian is given by

$$\mathcal{L} \supset \mathcal{L}_S + \mathcal{L}_\chi - V(S,\Phi), \tag{2.2}$$

[2]Besides the minimal model we consider in this study, there are two minimal classes of models, depending on how the scalar mediator transforms under $SU(2)_L$ and on the hypercharge assignments of the scalar mediator. For instance, the scalar mediator may carry the same quantum numbers as a right-handed down-type quark. In this case, there is no influence on the top-quark FCNC decays at the one-loop order, but only on the rates of the FCNC decays of the SM Higgs boson. In the other scenario, the scalar mediator belongs to a doublet under $SU(2)_L$, which would therefore impact the top-quark FCNC transitions, Higgs boson decays into $b\bar{s}$, and low-energy B-meson FCNC decays.

where $\mathcal{L}_S$, $\mathcal{L}_\chi$, and $V(S,\Phi)$ refer to the kinetic Lagrangian of the mediator, the Yukawa-type Lagrangian of the DM particle, and the scalar potential, respectively. The first two Lagrangian terms are given by

$$\mathcal{L}_S + \mathcal{L}_\chi \equiv i\bar{\chi}\partial\chi^c + \frac{1}{2}M_\chi\bar{\chi}\chi^c + (\mathcal{D}_\mu S)^\dagger(\mathcal{D}^\mu S) + (Y_q\bar{q}_R^c\chi S^\dagger + \text{H.c.}), \tag{2.3}$$

where the first and second terms refer to the kinetic energy and mass terms of the right-hand fermion, the third term refers to the gauge-invariant kinetic term of the scalar mediator, and the last term corresponds to the $S\chi q$ interaction (where a sum over the quark generations is implicit). In Eq. (2.3), $Y_q, q = u,\ c,\ t$ are generation-dependent Yukawa-type couplings, and $\mathcal{D}_\mu$ is the covariant derivative given by

$$\mathcal{D}_\mu = \partial_\mu - ig_s T^a G_\mu^a - \frac{g_1}{2}Y_S B_\mu,$$

with $T^a = \lambda_1^a/2$ being the generators of $SU(3)_c$. Y_S is the hypercharge of the scalar mediator, while g_1 and g_s are the coupling constants of the $U(1)_Y$ and $SU(3)_c$ gauge groups, respectively. Unless stated explicitly in the text, we assume that the DM Yukawa-type couplings are universal in the sense that $Y_u = Y_c = Y_t$. In the last term of the Lagrangian in Eq. (2.3), one can see that only one scalar mediator couples to all the SM quark generations. Therefore, one can generate top-quark FCNC decays at the one-loop order mediated *solely* by the dark particles of the model.[3] Assuming CP conservation, the most renormalizable and gauge-invariant scalar potential is given by

$$V(S,\Phi) = -m_{11}^2|\Phi^\dagger\Phi| + m_{22}^2|S^\dagger S| + \lambda_1|\Phi^\dagger\Phi|^2 + \lambda_2|S^\dagger S|^2 + \lambda_3|S^\dagger S||\Phi^\dagger\Phi|. \tag{2.4}$$

Here, $\Phi = (0,(v+H)/\sqrt{2})^T$ refers to the SM Higgs doublet given in the unitary gauge. All the parameters in the scalar potential are assumed to be real-valued parameters. Note that the quartic coupling λ_2 does not influence the phenomenology of the model, and henceforth it will be set to be equal to 1. On the other hand, λ_3 is subject to constraints from $H \to gg$ and $H \to \gamma\gamma$ signal-strength measurements. The effects of the model parameters on the Higgs decay observables is shown in Appendix A. Note that in this model, the contribution to the ρ parameter is exactly zero, as shown in Appendix B. We close this section with a discussion of the decays of the colored mediator (S) in this model. The partial decay width of S into χq is given by

$$\Gamma(S \to q\chi) \equiv \frac{Y_q^2 M_S}{16\pi}\left(1 - \frac{M_\chi^2 + m_q^2}{M_S^2}\right)\sqrt{\lambda\left(1, \frac{M_\chi^2}{M_S^2}, \frac{m_q^2}{M_S^2}\right)}, \approx \frac{Y_q^2 M_S}{16\pi}\left(1 - \frac{M_\chi^2}{M_S^2}\right)^2, \qquad m_q \ll M_S, \tag{2.5}$$

where $\lambda(x,y,z) \equiv x^2 + y^2 + z^2 - 2(xy + xz + yz)$ is the Källen function. A few comments are in order here. First, for $\Delta \equiv M_S - M_\chi \leq m_t$, the scalar mediator decays *solely* to an up quark or a charm quark plus χ, with branching ratios satisfying

$$\frac{\text{BR}(S \to u\chi)}{\text{BR}(S \to c\chi)} \approx \left(\frac{Y_u}{Y_c}\right)^2. \tag{2.6}$$

Once Δ becomes larger than the top-quark mass, the decay $S \to t\chi$ opens up with a branching starting from a few percent near the threshold and becoming very significant for $M_S \gg m_t$. Note that these features are very important in connection with DM phenomenology and collider studies, as we will see in later sections.

III. TOP-QUARK FCNC DECAYS

In this work, we consider the FCNC two-body decays of the top quark into qZ and qH, where q refers to either an up quark or a charm quark. They are mediated by the loops of the scalar mediator and the DM particle, as we can clearly see in Fig. 1. The generic expression of the effective operators for the $t \to qZ$ and $t \to qZ$ decays, with $q = u, c$, is given by

$$-\mathcal{L}_{\text{eff}} = \bar{t}\gamma^\mu(f_{tqZ}^L P_L + f_{tqZ}^R P_R)qZ_\mu + \bar{t}p^\mu(g_{tqZ}^L P_L + g_{tqZ}^R P_R)qZ_\mu + \bar{t}(f_{tqH}^L P_L + f_{tqH}^R P_R)qH + \text{H.c.}, \tag{3.1}$$

where $f_{tqX}^{L,R}(X = Z, H)$ and $g_{tqZ}^{L,R}$ are form factors that are calculable at the one-loop order, $P_{L,R} = (1 \mp \gamma_5)/2$ are the projection operators, and p^μ is the four-momentum vector of the decaying top quark.

The expressions of the one-loop induced form factors are found using FeynArts version 3.11 [62] and FormCalc version 9.9 [63], while their numerical evaluations have been performed using LoopTools version 2.16 [64]. The form factors for $t \to qH$ are given by

[3]We must stress that although the Yukawa-type interaction in Eq. (2.3) is similar to the interaction of a right-handed squark with an up-type quark and a neutralino in supersymmetric models, the origin of top-quark FCNC decays is completely different from the case of, e.g., the MSSM. In the MSSM, the main contributions come from loops of chargino-neutralinos, gluino-squarks, or the charged Higgs boson of the second doublet (see, e.g., Ref. [13]), while in our model there is only a neutralino-squark contribution. The simplicity of the model makes the connection between the dark matter and top-quark sectors very transparent, with tests of these predictions that can be easily performed at the HL-LHC.

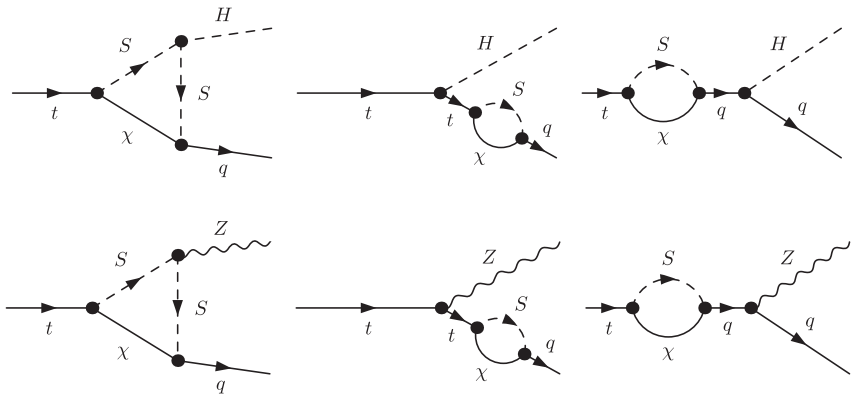

FIG. 1. Examples of Feynman diagrams for the $t \to qH$ (upper panel) and $t \to qZ$ (lower panel) decays.

$$f^L_{tqH} = \frac{Y_q Y_t m_t}{16\pi^2}\left(3\lambda_3 v C_1 + \frac{m_q^2}{v(m_t^2 - m_q^2)}(B_{1,t} - B_{1,q})\right),$$
$$f^R_{tqH} = \frac{Y_q Y_t m_q}{16\pi^2}\left(3\lambda_3 v C_2 + \frac{m_t^2}{v(m_t^2 - m_q^2)}(B_{1,t} - B_{1,q})\right), \tag{3.2}$$

while for $t \to qZ$, the form factors are given by

$$f^L_{tqZ} = \frac{g_1 m_q m_t (3c_W^2 - s_W^2)}{96 s_W \pi^2}\frac{Y_q Y_t}{(m_t^2 - m_q^2)}(B_{1,t} - B_{1,q}),$$
$$f^R_{tqZ} = -\frac{g_1 s_W Y_q Y_t}{24\pi^2}\left(2C_{00} + \frac{1}{m_t^2 - m_q^2}(m_t^2 B_{1,t} - m_q^2 B_{1,q})\right),$$
$$g^L_{tqZ} = \frac{g_1 s_W Y_q Y_t m_t}{12\pi^2}(C_1 + C_{11} + C_{12}),$$
$$g^R_{tqZ} = \frac{g_1 s_W Y_q Y_t m_q}{12\pi^2}(C_2 + C_{12} + C_{22}). \tag{3.3}$$

In Eqs. (3.2) and (3.3), $B_{1,Q} \equiv B_1(m_Q^2, M_\chi^2, M_S^2)$ and $C_{i,ij} \equiv C_{i,ij}(m_t^2, M_X^2, m_q^2, M_\chi^2, M_S^2, M_S^2)$ refer to the two-point and three-point Passarino-Veltman scalar loop functions [65]. Here, $M_X = m_H$ for $t \to qH$ and $M_X = M_Z$ for $t \to qZ$. It is clear from Eqs. (3.2) and (3.3) that $f^L_{tqH} \gg f^R_{tqH}$ and $f^R_{tqZ} \simeq g^L_{tqZ} \gg g^R_{tqZ} > f^L_{tqZ}$ given the mass dependence of these form factors. This can clearly be seen in Fig. 2, where we show the absolute values of the form factors as a function of the DM mass (M_χ) for three different values of the mass splitting $\Delta \equiv M_S - M_\chi$. We have checked that our results are free of UV divergences and independent of the nonphysical renormalization scale.[4]

Neglecting light quark masses, the resulting decay widths for $t \to qH$ and $t \to qZ$ are given by

$$\Gamma(t \to qH) = \frac{m_t}{32\pi}\left(1 - \frac{m_H^2}{m_t^2}\right)^2 |f^L_{tqH}|^2,$$
$$\Gamma(t \to qZ) = \frac{1}{16\pi m_t}\left(1 - \frac{M_Z^2}{m_t^2}\right)[\kappa_1 |f^R_{tcZ}|^2 + \kappa_2 |g^L_{tcZ}|^2 - 2\kappa_3 \mathrm{Re}(g^L_{tcZ} f^{R,*}_{tcZ})], \tag{3.4}$$

with κ_1, κ_2, and κ_3 being functions of m_t and M_Z:

$$\kappa_1 \equiv \frac{m_t^4}{2M_Z^2}\left(1 + \frac{m_t^2}{M_Z^2} - \frac{2M_Z^4}{m_t^4}\right),$$
$$\kappa_2 \equiv \frac{m_t^2}{8M_Z^2}\left(1 - \frac{M_Z^2}{m_t^2}\right) \times (m_t^2 - M_Z^2)^2,$$
$$\kappa_3 \equiv \frac{m_t}{4M_Z^2}(m_t^2 - M_Z^2)^2.$$

Note that the inclusion of the light-quark mass effects would induce a correction that is below 0.1% to the partial widths of the top quark. The resulting branching ratios are given by

$$\mathrm{BR}(t \to qX) = \frac{\Gamma(t \to qX)}{\Gamma_t}, \tag{3.5}$$

where $\Gamma_t \equiv \Gamma(t \to bW) = 1.32$ GeV calculated at next-to-next-to-leading order in QCD, including the finite mass and width effects and next-to-leading order electroweak corrections [67]. We note that our model predicts that

$$\frac{\Gamma(t \to cX)}{\Gamma(t \to uX)} \approx \left(\frac{Y_c}{Y_u}\right)^2,$$

since the m_q^2 corrections to the FCNC partial widths are extremely small. This model predicts a ratio

$$\frac{\Gamma(t \to qZ)}{\Gamma(t \to qH)} \approx \frac{r}{\lambda_3^2}, \tag{3.6}$$

[4]Note that this finding holds true only for the case of on-shell particles in the initial/final state. For the off-shell case, a more refined treatment of the renormalization needs to be adopted (see, e.g., Ref. [66]).

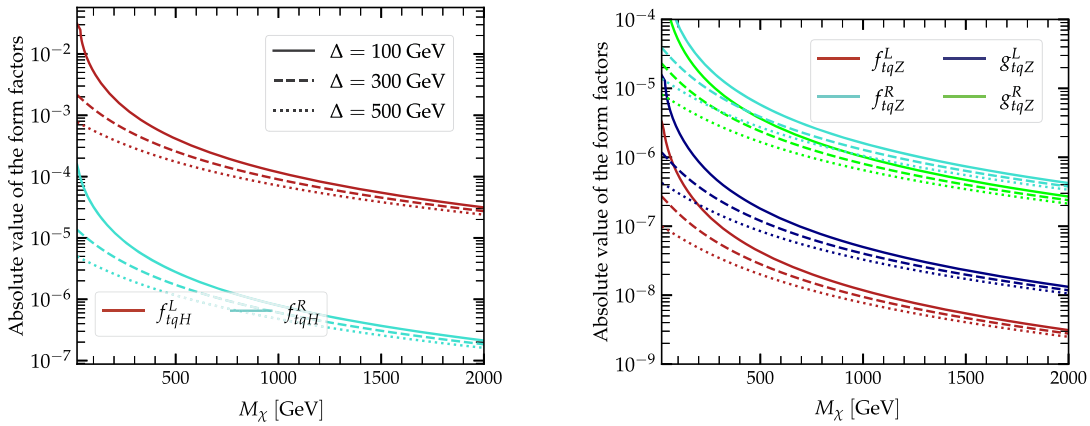

FIG. 2. The absolute value of the form factors for $t \to qH$ (left) and $t \to qZ$ (right) as a function of M_χ for $\Delta = 100$ GeV (solid lines), $\Delta = 300$ GeV (dashed lines) and $\Delta = 500$ GeV (dash-dotted lines). Here, we assume that the light quark q is the charm quark, and we take $Y_c = Y_t = 1$ and $\lambda_3 = 1$.

where r is a factor that depends on the DM mass and the mass splitting (Δ) and varies between 5 and 15. We find that r is smaller for high M_χ and higher for small M_χ.

In Fig. 3, we display the branching ratios of $t \to qH$ (left) and of $t \to qZ$ (right) as a function of M_χ for different values of the mass splitting Δ and of the Yukawa-type coupling $Y_q = Y_t$. Here, we show the results for $Y_q = 1$, 2, and 3 with the choices of $\Delta = 100$ GeV (turquoise), $\Delta = 300$ GeV (blue), and $\Delta = 500$ GeV (purple). These two FCNC branching ratios scale as $|Y_q Y_t|^2$, and therefore higher values of $Y_q = Y_t$ will lead to extremely large branching ratios, especially for small M_χ and small Δ. We also show the experimental bounds reported on by ATLAS [41] and CMS [47] as horizontal solid (for $t \to uX$) and dashed (for $t \to cX$) lines. The strong bounds from the search of $t \to qZ$ imply that DM masses of order 400 GeV are excluded at the 95% CL if one assumes that $\Delta = 100$ GeV and $Y_q = 3$. Smaller values of the DM mass are still allowed if one considers $Y_q \approx 1$ and relatively large Δ. On the other hand, we can see that for heavy DM with mass $M_\chi \geq 1000$ GeV, the branching ratios become relatively independent of the choice of Δ.

IV. DARK MATTER

The relic density of the χ particles is mainly due to the freeze-out mechanism. The main process that leads to DM

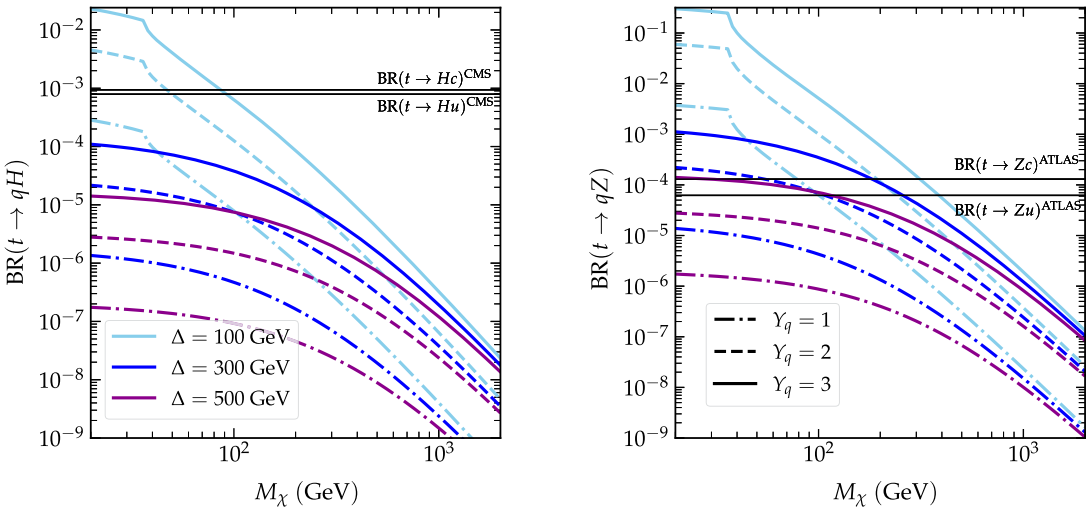

FIG. 3. The FCNC decay branching ratios as a function of the dark matter mass (M_χ) for $t \to qH$ (left) and $t \to qZ$ (right). The results are shown for $Y_q = 1$ (dash-dotted lines), $Y_q = 2$ (dashed lines), and $Y_q = 3$ (solid lines). For each case, we calculate the branching ratios for $\Delta = 100$ GeV (turquoise), $\Delta = 300$ GeV (blue), and $\Delta = 500$ GeV (purple). For $t \to qH$, we choose $\lambda_3 = 1$. We also display the latest exclusion bounds from the searches of the FCNC production of top quarks reported on by the ATLAS [41] and CMS [47] collaborations. More details can be found in the text.

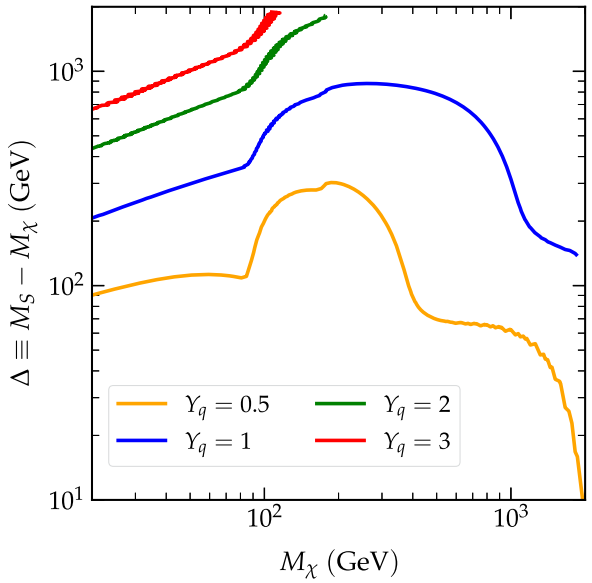

FIG. 4. Parameter space satisfying $\Omega_\chi h^2 = 0.12$ shown in the (M_χ, Δ) plane. The thin solid curves are corresponding to contours of constant coupling $Y_q = 0.5$ (orange), $Y_q = 1$ (blue), $Y_q = 2$ (green), and $Y_q = 3$ (red), where $Y_q \equiv Y_u = Y_c = Y_t$.

relic density within this model is through the annihilation into $q_\alpha \bar{q}_\beta$, where α and β are generation indices. This includes the case of same-flavor production $(u\bar{u}, c\bar{c}, t\bar{t})$ and of different-flavor production $(u\bar{c}, c\bar{u}, u\bar{t}, t\bar{u}, c\bar{t}, c\bar{u})$. The coannihilation channels start to dominate for small mass splittings between the χ particle and the colored mediator S. The DM density of the χ particles can be obtained by solving the following Boltzmann equation, assuming that the colored mediator has already decayed into $\chi + q_\alpha$:

$$\frac{\mathrm{d}n}{\mathrm{d}t} = -3Hn - \langle \sigma_{\mathrm{eff}} v(x_f) \rangle (n^2 - n_{\mathrm{eq}}^2), \tag{4.1}$$

where H is the Hubble parameter, $\langle \sigma_{\mathrm{eff}} v(x_f) \rangle$ is the thermally averaged annihilation cross section of DM with a velocity v at the freeze-out temperature x_f, and n_{eq} is the equilibrium number density.

An approximate solution of the Boltzmann equation leads to the following expression for the DM relic density [68–70]:

$$\Omega_\chi h^2 \simeq \frac{1.04 \times 10^9}{M_{\mathrm{Planck}}} \frac{x_f}{\sqrt{g_*(x_f)}} \frac{1}{I_a + 3\frac{I_b}{x_f}}, \tag{4.2}$$

where $M_{\mathrm{Planck}} = 1.22 \times 10^{19}$ GeV is the Planck mass, g_* is the effective number of degrees of freedom, and I_a and I_b are coefficients that depend on the effective cross section. Here, I_a is related to the velocity-independent cross section, and I_b is related to the velocity-dependent cross section (see, e.g., Ref. [70] for more details). We assume that the thermally averaged cross section can be expanded as

$$\sigma_{\mathrm{eff}} v = a_{\mathrm{eff}} + b_{\mathrm{eff}} v^2 + \mathcal{O}(v^4), \tag{4.3}$$

where the expression of a_{eff} and b_{eff} can be found in, e.g., Ref. [70]. In this analysis, we use micrOMEGAs version 5.3.41 [71] to solve numerically the Boltzmann equations and to calculate the relic density of the χ particles. We have cross-checked the results of micrOMEGAs by comparing them with the results of MadDM version 3.1 [72] for various benchmark points. The results of the calculations are shown in Fig. 4, where the couplings satisfying the condition $\Omega_\chi h^2 = 0.12$ are shown in the plane of M_χ and $\Delta = M_S - M_\chi$. We show the contours for $Y_q = 0.5$ (orange), $Y_q = 1$ (blue), $Y_q = 2$ (green), and $Y_q = 3$ (red). We can see that in order to fulfill the correct relic density, reasonably modest to large values of Y_q are required, which increase with increasing mass splitting Δ. On the other hand, we can see that there is a wide peak for DM masses above ≈80 GeV for a given value of the DM coupling, which indicates the opening of the annihilation channel $\chi\chi \to t\bar{t}$. Finally, we note that the effect of coannihilation[5] becomes very important for small Δ and large M_χ.

We turn now to a brief discussion of the prospects of DM indirect detection within this model. The main annihilation channels, as pointed out previously, are into $q_\alpha \bar{q}_\beta$, which can be either same-flavor or different-flavor quarks. In the selected benchmark points, the main DM annihilation channels are the ones corresponding to different quarks $(c\bar{u}, c\bar{t}, u\bar{t})$, for which no tabulated spectra for the particle fluxes at the production exist. Therefore, a more detailed analysis may become relevant in a future work.

We close this section by commenting on the effects of DM direct-detection searches on the model parameter space. In this model, the spin-independent nucleus-DM scattering cross section (σ_{SI}) gets contributions from both the tree-level (left panel of Fig. 5) and the NLO RGE-improved (middle and right panels of Fig. 5). The spin-independent cross section takes the generic form

[5]We must stress that in some model configurations, the effect of both Sommerfeld enhancement and bound-state formation on the DM relic density can be important. These effects have been studied in great detail in Ref. [60] within similar t-channel simplified models. It is found that, for t-channel models where the mediator has the same quantum numbers as the right-handed up-type quark, the corrections from Sommerfeld enhancement are very small for the DM masses we considered in this study unless the DM coupling is of order $g_{\mathrm{DM}} \approx \mathcal{O}(10^{-2})$ (see the upper panel of Fig. 4 in Ref. [60]).

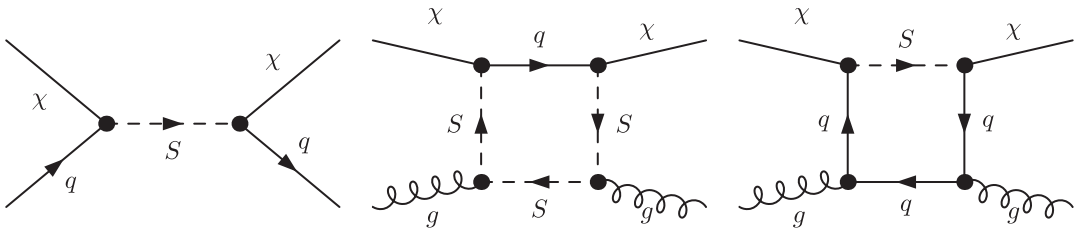

FIG. 5. Examples of Feynman diagrams contributing to the spin-independent DM-nucleus cross section at tree level (left panel) and at the NLO (middle and right panels).

$$\sigma_{\rm SI} \equiv \frac{4}{\pi}\left(\frac{M_\chi m_N}{M_\chi + m_N}\right)^2 |f_N|^2, \tag{4.4}$$

where m_N is the nucleus mass and f_N is the form factor which encodes all the model-dependent, nuclear, and QCD corrections. In this work, we only perform the calculations of $\sigma_{\rm SI}$ using micrOMEGAs [71]. A more detailed NLO analysis of the bounds from the spin-independent cross section has been done in, e.g., Refs. [57,60,73]. It has been found by the authors of Ref. [57] that the NLO and RGE-improved corrections induce an enhancement factor of about 4 on $\sigma_{\rm SI}$. Using these findings, we find that the benchmark points presented in Table II are still allowed by the current Xenon1T bounds, since BP1 is in the ballpark of the exclusion curve, while the other three benchmark points lead to values of $\sigma_{\rm SI}$ that are 1 or 2 orders of magnitude smaller than the current Xenon1T bound.

V. BOUNDS FROM THE LHC SEARCHES

The model predicts the production of DM at the LHC through a variety of processes leading to various final-state signatures such as monotop ($t + E_T^{\rm miss}$), $t\bar{t} + E_T^{\rm miss}$, monojet, and multijet + $E_T^{\rm miss}$. There are several collider studies on the models with t-channel mediators [58,59,61]. In these analyses, the scalar mediator is assumed to couple to one generation of quarks only. Therefore, constraints from multijet + $E_T^{\rm miss}$ are found to be strong, excluding a wide range of the parameter space [59]. In this model, we find that the strongest bound comes from the search of monojets

TABLE II. Definition of the benchmark points. Here, we show the branching ratios BR($S \to \chi q$) along with the width-to-mass ratio (Γ_S/M_S) of S. The FCNC branching ratios of the top quark, BR($t \to qH$) and BR($t \to qZ$), are also shown. For each benchmark point, we display the energy scale, denoted by $\Lambda_{\rm pole}$, at which the perturbativity bound is violated at the one-loop order (more details about the renormalization group equation can be found in Appendix C).

Benchmark point	Quantity	BP1	BP2	BP3	BP4
Parameters	Y_u	0.4	0.4	0.0	0.4
	Y_c	0.4	0.8	1.0	1.0
	Y_t	0.4	1.2	2.0	0.8
	λ_3	2.0	1.0	1.0	4.0
	M_χ (GeV)	500	200	100	600
	Δ (GeV)	57	650	500	250
	$\Lambda_{\rm pole}$ (TeV)	56	100	10	5.5
Branching ratios					
BR($S \to q\chi$)	BR($S \to u\chi$)	5.00×10^{-1}	7.60×10^{-2}	0.00×10^{0}	1.01×10^{-1}
	BR($S \to c\chi$)	5.00×10^{-1}	3.03×10^{-1}	2.31×10^{-1}	6.32×10^{-1}
	BR($S \to t\chi$)	0.00×10^{0}	6.21×10^{-1}	7.69×10^{-1}	2.67×10^{-1}
	Γ_S/M_S	1.18×10^{-4}	3.64×10^{-2}	8.31×10^{-2}	7.92×10^{-3}
BR($t \to qX$)	BR($t \to cH$)	1.02×10^{-8}	1.98×10^{-8}	3.69×10^{-7}	1.43×10^{-7}
	BR($t \to uH$)	1.02×10^{-8}	4.95×10^{-9}	0.0	2.29×10^{-8}
	BR($t \to cZ$)	1.50×10^{-8}	1.79×10^{-7}	3.49×10^{-6}	5.92×10^{-8}
	BR($t \to uZ$)	1.50×10^{-8}	4.48×10^{-8}	0.0	9.48×10^{-9}

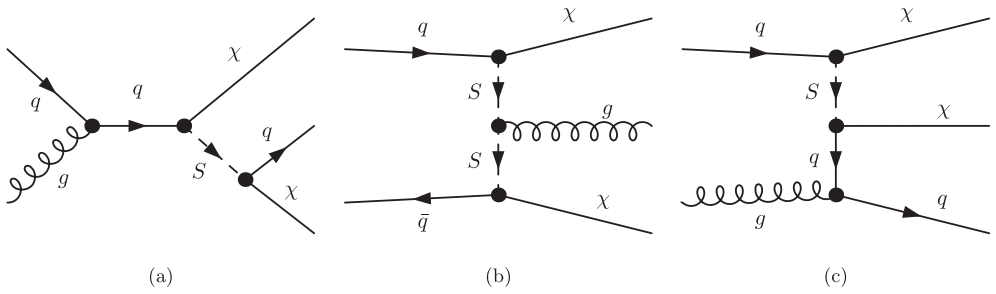

FIG. 6. Representative Feynman diagrams for monojet production in this model. Here, we show the monojet production through (a) resonant $S\chi$ production and (b),(c) nonresonant production.

(small number of jets and missing energy) which was carried out by the ATLAS Collaboration [75].[6] Examples of Feynman diagrams for monojet production in this model at leading order (LO) are shown in Fig. 6. In this model, one can distinguish between resonant production [Fig. 6(a)] and nonresonant production through $q\bar{q}$ annihilation [Fig. 6(b)] and through qg fusion [Fig. 6(c)]. The cross section of the monojet production can be generically expressed as follows:

$$\sigma(pp \to \chi\chi J) \equiv \sum_{i,j} \int \mathrm{d}x_i \mathrm{d}x_j f_{i/p}(x_i, Q^2) \times f_{j/p}(x_j, Q^2)\hat{\sigma}(ij \to \chi\chi J). \quad (5.1)$$

Here, $f_{i/p}(x_i, Q^2)$ is the PDF of a parton i within the proton to carry a momentum fraction x_i at a factorization scale Q, and $\hat{\sigma}$ is the partonic cross section which scales in this process as $\hat{\sigma}(ij \to \chi\chi J) \propto Y_q^4$. Here, Y_q is either Y_u or Y_c. Note that for all the diagrams, the contribution of the charm quark PDF is always smaller than the contribution of the up or down quarks. The analysis we consider in this study targeted the search of new physics beyond the Standard Model in final states consisting of a small number of jets in association with missing energy using 139 fb^{-1} of data collected in the period of 2015–2018. In this analysis, events are required to have at least one jet with a transverse momentum of 150 GeV and no reconstructed isolated "loose" electrons or muons with $p_T > 7$ GeV and $|\eta| < 2.5$, tau leptons with $p_T > 10$ GeV and $|\eta| < 2.5$, or photons with $p_T > 10$ GeV and $|\eta| < 2.5$. The missing transverse energy (E_T^{miss}) is required to be larger than 200 GeV. Twenty-six signal regions are defined depending on the cut on E_T^{miss}: 13 inclusive signal regions (IM0–IM12), and 13 exclusive signal regions (EM0–EM12).

To estimate the bounds on the model parameter space arising from this search, we use a validated implementation, which is denoted by ATLAS-EXOT-2018-06, in the MadAnalysis 5 framework [76–79]. The link to the analysis code along with the validation material can be found in Ref. [80]. Theory predictions for the signal have been made using MadGraph5_aMC@NLO version 3.5.0 [81] with leading order (LO) matrix elements. The matrix elements have been convoluted with the NNPDF31_lo_as_0130 PDF set with $\alpha_s(M_Z) = 0.130$ [82], which can be found in LHAPDF version 6.4.0 [83]. Note that our choice of α_s is adopted to capture some of the missing higher-order corrections, although the calculation is only accurate at LO. The generated events are then interfaced to PYTHIA 8 version 8309 [84] to add parton showering and hadronization. All the jets were clustered with the anti-k_t algorithm with a jet radius of $R = 0.4$ [85] using FastJet version 3.40 [86]. Simplified detector modeling was achieved with the use of the simplified fast-detector simulation (SFS) module of MadAnalysis 5 [87]. To estimate the exclusion bounds on the model, we calculate the $\mathrm{CL_s}$ using Pyhf [88]. A point in the model parameter space is excluded at 95% if $\mathrm{CL_s} > 0.95$. In Fig. 7, we show the 95% confidence-level exclusions

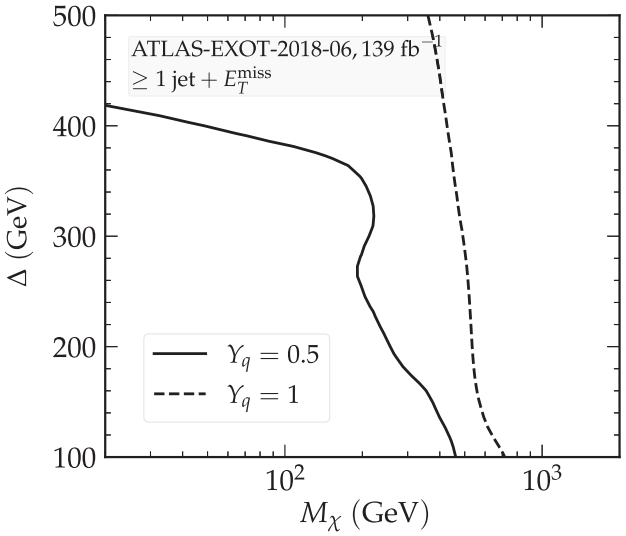

FIG. 7. The 95% CL exclusion on the model projected on the plane of (M_χ, Δ) for $Y_q = 0.5$ (solid line) and Y_q (dashed line). For the two cases, the contours correspond to $\mathrm{CL}_s^{95\%}$, which defines the exclusions at the 95% confidence level. Here, we assume that $Y_q = Y_u = Y_c$ for simplicity.

[6]A comprehensive analysis of all the existing collider searches at the LHC will be performed in a future study.

TABLE III. Some characteristics of the benchmark scenarios to be considered for future collider analyses.

Benchmark point	Quantity	BP1	BP2	BP3	BP4
Dark matter	$\Omega_\chi h^2$	1.18×10^{-1}	6.42×10^{-2}	8.58×10^{-2}	1.05×10^{-1}
	$\sigma^p_{\rm SI}$ (cm^2)	4.74×10^{-47}	3.51×10^{-50}	4.57×10^{-49}	2.97×10^{-48}
Production cross sections [fb]					
13.6 TeV	$S\chi$	6.11×10^{1}	3.23×10^{1}	7.89×10^{1}	1.34×10^{1}
	$SS^\dagger$	1.56×10^{2}	1.19×10^{1}	1.06×10^{2}	1.16×10^{1}
	SS + H.c.	1.79×10^{1}	1.45×10^{0}	4.80×10^{-1}	5.47×10^{0}
	$\chi\chi H$	3.36×10^{-4}	2.65×10^{-4}	9.00×10^{-4}	4.94×10^{-4}
	$\chi\chi Z$	1.82×10^{-3}	1.25×10^{-2}	1.48×10^{-2}	2.08×10^{-3}
	χSH	5.35×10^{-2}	3.85×10^{-3}	1.11×10^{-2}	3.02×10^{-2}
	χSZ	4.44×10^{-2}	2.27×10^{-2}	3.88×10^{-2}	1.12×10^{-2}
	$SS^\dagger j$	2.19×10^{2}	1.64×10^{1}	1.46×10^{2}	1.63×10^{1}
	$SS^\dagger \gamma$	1.02×10^{0}	1.10×10^{-1}	7.40×10^{-1}	1.10×10^{-1}
	$SS^\dagger t$	8.21×10^{-2}	1.40×10^{-1}	1.01×10^{0}	4.50×10^{-2}
	$SS^\dagger H$	4.80×10^{-1}	6.42×10^{-3}	7.69×10^{-2}	1.00×10^{-1}
	$SS^\dagger Z$	2.40×10^{-1}	2.85×10^{-2}	1.80×10^{-1}	2.86×10^{-2}
100 TeV	$S\chi$	3.41×10^{3}	2.32×10^{3}	6.53×10^{3}	1.57×10^{3}
	$SS^\dagger$	28.82×10^{3}	4.63×10^{3}	21.36×10^{3}	4.61×10^{3}
	SS + H.c.	2.25×10^{2}	4.94×10^{1}	5.39×10^{1}	2.31×10^{2}
	$\chi\chi H$	1.61×10^{-2}	1.01×10^{-2}	5.09×10^{-2}	4.69×10^{-2}
	$\chi\chi Z$	9.91×10^{-2}	5.03×10^{-1}	8.84×10^{-1}	2.04×10^{-1}
	χSH	4.32×10^{0}	4.07×10^{-1}	1.39×10^{0}	5.06×10^{1}
	χSZ	4.24×10^{0}	2.27×10^{0}	5.35×10^{0}	2.26×10^{0}
	$SS^\dagger j$	58.65×10^{3}	10.36×10^{3}	43.92×10^{3}	10.32×10^{3}
	$SS^\dagger \gamma$	1.38×10^{2}	2.48×10^{1}	8.91×10^{1}	2.75×10^{1}
	$SS^\dagger t$	1.38×10^{1}	6.65×10^{1}	3.73×10^{2}	2.25×10^{1}
	$SS^\dagger H$	1.28×10^{2}	3.64×10^{0}	2.24×10^{1}	5.84×10^{1}
	$SS^\dagger Z$	2.65×10^{1}	6.66×10^{0}	2.16×10^{1}	6.70×10^{0}

projected on the plane of (M_χ, Δ) for two assumptions on the coupling: $Y_q = 0.5$ (solid) and $Y_q = 1$ (dashed). We can see that for $Y_q = 1$ DM, masses up to 800 GeV are excluded, with very small dependence on the mass splitting (Δ). However, for the choice of $Y_q = 0.5$, the bounds get weaker, given that the total cross section behaves approximately as Y_q^4. Note that further improvements on the bounds can be made if one considers calculations at NLO (see Ref. [58] for more details). We plan to improve our results in a future work [89].

VI. BENCHMARK SCENARIOS FOR FUTURE COLLIDER ANALYSES

In this section, we present four benchmark points consistent with the current experimental bounds from LHC searches of new physics, top-quark FCNC decays, Higgs boson couplings and cosmology. We also show the production rates for several processes which may be amenable to discovery at either the HL-LHC or the FCC-hh. The definition of the benchmark points is shown in Table II, including the decay branching ratios of the colored scalar mediator and the top-quark FCNC. Given the importance of the choice of λ_3 in our model, we also show the energy scale at which the perturbativity of the model is broken down (more details about the RGEs are shown in Appendix C). Some of the characteristics of the benchmark points are shown in Table III. We give a few comments about the benchmark points[7]:

BP1. This benchmark point is characterized by two main properties. First, all the Yukawa-type couplings (Y_q) are chosen to be equal—i.e., $Y_u = Y_c = Y_t = 0.4$. Second, we have chosen a small mass splitting between χ and S; $\Delta = 57$ GeV. For this choice of M_χ, the dominant contribution to the relic abundance comes from the coannihilation mechanism. We list the channels by their contribution to $(\Omega_\chi h^2)^{-1}$: $\chi S \to qg, qH, t$ contribute by about 65%; $\chi\chi \to q_\beta \bar{q}_\alpha$ contributes by about 21%; and $SS^\dagger \to W^+W^-, gg$ contribute by about 7%. Given that the mass splitting is smaller than the top-quark mass, the main decay channel of S is into $u\chi$ and $c\chi$ with an equal branching ratio of 50%

[7]We expect that constraints from flavor observables such as in D^0-$\bar{D}^0$ oscillation are expected to be small in our model since the leading contribution occurs through dimension-six SMEFT operators suppressed by loop and mass factors ($\sim M_S^{-2} M_\chi^{-2}$).

for each channel. The choice of $Y_u = Y_c$ leads to $\mathrm{BR}(t \to uX) = \mathrm{BR}(t \to cX)$, while the choice of $\lambda_3 = 2$ implies that $\mathrm{BR}(t \to qZ) \approx 1.5 \times \mathrm{BR}(t \to qH)$. For this benchmark point, we find that the best channels to look for are the production of $\chi\chi$ in association with jets: $S(\to j\chi)\chi$, $S(\to j\chi)S^\dagger(\to j\chi)$, $S(\to j\chi)S^\dagger(\to j\chi)j$, and $S(\to j\chi)S^\dagger(\to j\chi)H(\to b\bar{b})$, where $j = u, \bar{u}, c, \bar{c}$. There is also an important process to search for at hadron colliders, which is the production of $SS^\dagger\gamma$ which leads to final states comprising at least 2 jets, a high-p_T photon, and large missing energy.

BP2. Here, we choose a normal hierarchy for the couplings—i.e., $Y_t > Y_c > Y_u$. Large mass splitting ($\Delta = 650$ GeV) and a relatively light DM ($M_\chi = 200$ GeV) are chosen. Given this large mass splitting, the DM relic density is mainly due to the annihilation mechanism, where annihilation into $t\bar{t}$ and $c\bar{t} + t\bar{c}$ contribute to the relic density by 55% and by 34%, respectively. In this benchmark scenario, the relic density of the χ particles forms about 53% of the total DM relic density in the Universe. On the other hand, the top-quark FCNC branching ratios satisfy $\mathrm{BR}(t \to cX) \approx 4 \times \mathrm{BR}(\to uX)$ and $\mathrm{BR}(t \to qZ) \approx 9.04 \times \mathrm{BR}(t \to qH)$. Due to this choice of couplings, the S particle decays dominantly into $t\chi$ with a BR of 62.1%, followed by $S \to c\chi$ with a BR of 30.3%, while the decay $S \to u\chi$ is subleading with a BR smaller than 10%. In this scenario, processes involving one top quark or more in association with large missing energy are the most prominent at hadron colliders. Here, five processes may lead to interesting signatures: $S(\to t\chi)\chi$, $S(\to t\chi)S^\dagger(\to \bar{t}\chi)$, $S(\to t\chi)S(\to t\chi) + \mathrm{H.c.}$,[8] $S(\to t\chi)S^\dagger(\to \bar{t}\chi)j$, and $S(\to t\chi) \times S^\dagger(\to \bar{t}\chi)t$. The latter channel is interesting, as it leads to final states of three top quarks and missing energy. There are other channels that involve the production of one or two hard jets initiated by u and c quarks in association with one or two top quarks.

BP3. In this benchmark point, we specifically choose the coupling to the u quark to be exactly zero and assume the other couplings to be $Y_t = 2 \times Y_c = 2$ and $\lambda_3 = 1$. For the particle masses, we choose a DM of mass 100 GeV and a mediator with a mass of 600 GeV. For this choice of mass and couplings, the most dominant decay of S is into $t\chi$ with a branching ratio of 76.9%, followed by the decay into $c\chi$ with a branching ratio of 23.1%. The relic density of the χ particle in this benchmark point is about 71.5% of the total DM relic density and is mainly due to the annihilation of χ into $c\bar{t} + t\bar{c}$ with a contribution of 92%. In this scenario, the branching ratios of $t \to uZ$ and $t \to uH$ are exactly zero, while the decays involving charm quarks satisfy $\mathrm{BR}(t \to cZ) \approx 9.46 \times \mathrm{BR}(t \to cH)$. In addition to processes like the production of one or two top quarks and jets in association with missing energy, this BP can be probed using processes involving Higgs bosons as well—i.e., $S(\to t\chi)S^\dagger(\to \bar{c}\chi)H$ and $\chi S(\to t\chi)H$. These two processes are advantageous, since they have smaller associated backgrounds and can be used to connect top FCNCs and DM at hadron colliders.

BP4. We select the couplings to satisfy $Y_c > Y_t > Y_u$ and $\lambda_3 = 4$. Moreover, we choose the DM to be quite heavy, with a mass of 600 GeV and a mass splitting of 250 GeV. The dominant decay of S is into $c\chi$ with a branching ratio of 62.3%, followed by $t\chi$ and $u\chi$ with branching ratios of 26.7% and 10.1%, respectively. The top FCNC decays into cX dominate over uX with branching ratios satisfying $\mathrm{BR}(t \to cX) \approx 6.24 \times \mathrm{BR}(t \to uX)$, where the proportionality factor is approximately equal to $(Y_c/Y_u)^2$. In this BP, the branching ratio of top FCNC decay into $H + q$ is larger than that into $Z + q$ and satisfies $\mathrm{BR}(t \to qH) \approx 2.41 \times \mathrm{BR}(t \to qZ)$. The relic density in this BP is mainly due to the annihilation of χ into $c\bar{t}$, $t\bar{c}$, $t\bar{t}$, and $c\bar{c}$, with a combined contribution of about 86%. This choice leads to $\Omega_\chi h^2/\Omega_{\mathrm{Planck}} h^2 \approx 87.1\%$. The heavy-DM scenario in this BP leads to smaller cross sections for the production of χ and S in hadron colliders as compared to the rates for the other BPs.

VII. CONCLUSIONS

In this work, we have suggested a minimal simplified model that simultaneously addresses the DM problem and generates *nonzero* rates for top-quark FCNC decays. In this model, the SM is extended by two $SU(2)_L$ singlets: a colored scalar mediator (S) that carries the same quantum numbers as a right-handed up-type quark, and a Majorana fermion (χ) which plays the role of the DM candidate. The two extra states are odd under an *ad hoc* Z_2 symmetry, which is imposed to guarantee the stability of χ, provided that $M_\chi \leq M_S$. Since the colored scalar mediator couples to all the quark generations, *nonzero* rates for top-quark FCNC decays are induced through the loops of S and χ. Using examples of two interesting top-quark FCNC decays—i.e., $t \to qH$ and $t \to qZ$—we have comprehensively analyzed the contribution of these two extra states on the corresponding branching ratios. First, we found that the top-quark FCNC branching ratios do not depend on the light quark masses, but only on their coupling to χ and S (denoted by Y_q). Second, we found that the branching ratios $\mathrm{BR}(t \to qH)$ and $\mathrm{BR}(t \to qZ)$ are related by phase-space factors and the coupling of S to the SM Higgs boson doublet. We then analyzed the DM relic density in this model, which is mainly due to the annihilation of the χ particles into quarks unless the mass splitting between χ and S is small, in which case coannihilation into SM particles starts to dominate. The bounds from the LHC searches of DM in monojet were analyzed. After analyzing all these constraints, we have defined four benchmark points that can lead to high discovery potential at the

[8]Note that the production of SS always dominates over $S^\dagger S^\dagger$, since its rate is initiated by valence u quarks.

HL-LHC and FCC-hh. We discussed in detail the characteristics of these benchmark points and the different methods to probe them at high-energy colliders. This work provides a novel interesting connection between top-quark FCNC, the DM problem, and collider searches of new physics BSM.

ACKNOWLEDGMENTS

The work of A. J. is supported by the Institute for Basic Science (IBS) under the Project Code IBS-R018-D1. The work of S. K. is supported by JSPS KAKENHI Grants No. 20H00160 and No. 23K17691. A. J. would like to thank the CERN Theory Department, where part of this work has been done, for its hospitality.

APPENDIX A: IMPACT ON HIGGS BOSON COUPLINGS

As pointed out in Sec. II, the Higgs boson couplings get contributions from the parameters of this model. Here, we show explicitly the impact of the Higgs measurements on the allowed range of the model's parameters. There are two different categories of decay channels that can be affected by this model: bosonic decays into $\gamma\gamma$ and gg, and fermionic decays into $u\bar{u}$ and $c\bar{c}$. In this appendix, we do not consider the contribution to bosonic decay processes like ZZ^* or WW^*, since it was found that they are small and do not go beyond a few percent; see Refs. [90–92]. The main aim of this section is to evaluate the following ratio:

$$\kappa_i = \sqrt{\frac{\Gamma(H \to i)}{\Gamma(H \to i)^{\rm SM}}}, \tag{A1}$$

where $i = g,\ \gamma,\ u,\ c$. We start with the bosonic decay channels. In this model, the new contribution to these decay widths depends solely on the mass of the colored mediator (M_S) and the quartic coupling (λ_3). The partial decay widths for the $\gamma\gamma$ and gg channels are given by

$$\begin{aligned}
\Gamma(H \to \gamma\gamma) &= \frac{G_F \alpha_{\rm EM}^2 m_H^3}{128\sqrt{2}\pi^3}\left|\sum_f Q_f^2 N_{cf} A_{1/2}(\tau_f) + A_1(\tau_W) + N_{cS} Q_S^2 \frac{\lambda_3 v^2}{2M_S^2} A_0(\tau_S)\right|^2, \\
\Gamma(H \to gg) &= \frac{G_F \alpha_s^2 m_H^3}{64\sqrt{2}\pi^3}\left|\sum_f A_{1/2}(\tau_f) + \frac{\lambda_3 v^2}{2M_S^2} A_0(\tau_S)\right|^2,
\end{aligned} \tag{A2}$$

with $N_{cX} = 3$ being the number of colors for the quarks and the scalar mediator. $\tau_i = m_H^2/(4m_i^2)$, $A_{1/2}(\tau) = 2\tau^{-2}(\tau + (\tau-1)f(\tau))$, $A_1(\tau) = -\tau^{-2}(2\tau^2 + 3\tau + 3(2\tau-1)f(\tau))$, $A_0(\tau) = -\tau^{-2}(\tau - f(\tau))$, and $f(\tau)$ is the one-loop function, which can be found in, e.g., Ref. [93]. In the SM, the contribution of the W boson to $\Gamma(H \to \gamma\gamma)$ is dominant as compared to the contribution of the top quark, and it comes with an opposite sign. The contribution of the colored scalar is mainly controlled by the value of λ_3. We can see that there is destructive (constructive) interference for positive (negative) values of λ_3 with the dominant W-boson contribution. The situation is different for the case of $H \to gg$, since the only dominant contribution in the SM is that of the top quark. The new scalar contribution comes with the same sign as the top-quark contribution for $\lambda_3 > 0$, leading to enhancement, while it reduces the rate of $H \to gg$ for negative λ_3. These features can be clearly seen in Fig. 8, where we show the dependence of κ_γ (left) and κ_g on M_S for different values of λ_3. We can see that κ_g and κ_γ are anticorrelated in this model, since, for example, the new scalar loops induce positive (negative) contributions[9] to κ_γ (κ_g) when $\lambda_3 < 0$. To compare with the experimental data, we also show the recent measurements of κ_γ and κ_g reported on by the ATLAS Collaboration [94]. We can see that the recent measurements of κ_γ and κ_g do not prefer light scalars, as masses of order 200–300 GeV are excluded for all but $\lambda_3 \approx 0$.

We turn now to a brief discussion of the contribution of the new states to the fermionic rates—i.e., $H \to u\bar{u}$ and $H \to c\bar{c}$. The partial width for these channels is given by

$$\Gamma(H \to q\bar{q}) \equiv \Gamma(H \to q\bar{q})_{\rm N3LO} + \Delta\Gamma(H \to q\bar{q})_{\rm NP}, \tag{A3}$$

where $\Gamma(H \to q\bar{q})_{\rm N3LO}$ is the decay width in the SM calculated at N3LO including renormalized running quark masses [95,96], and $\Delta\Gamma(H \to q\bar{q})_{\rm NP}$ is the model contribution to the decay width, which is given by

$$\Delta\Gamma(H \to q\bar{q})_{\rm NP} = \frac{6 m_H m_q}{16\pi v}[{\rm Re}(f_L + \delta f_L) + {\rm Re}(f_R + \delta f_R)], \tag{A4}$$

with $f_{L,R}$ being the one-loop form factors which depend on Y_q, λ_3, M_χ, and M_S, and they are given by

$$\begin{aligned}
f_L &= \frac{3\lambda_3 m_q v Y_q^2}{16\pi^2} C_2(m_q^2, m_H^2, m_q^2, M_\chi^2, M_S^2, M_S^2), \\
f_R &= \frac{3\lambda_3 m_q v Y_q^2}{16\pi^2} C_1(m_q^2, m_H^2, m_q^2, M_\chi^2, M_S^2, M_S^2).
\end{aligned} \tag{A5}$$

[9]The choice of a negative value of λ_3 may lead to vacuum configurations that break the color symmetry. Here, we only show the results for comparison, since an analysis of the color-breaking minima is beyond the scope of this work.

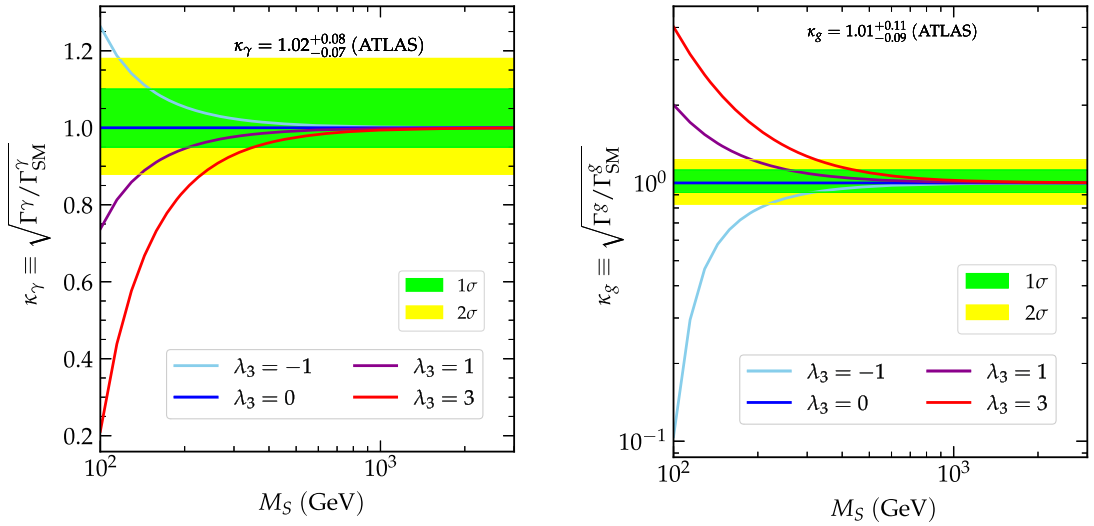

FIG. 8. The dependence of κ_γ (left) and κ_g (right) on the colored scalar mass (M_S) for $\lambda_3 = -1$ (turquoise), $\lambda_3 = 0$ (blue), $\lambda_3 = 1$ (purple), and $\lambda_3 = 3$ (red). In the same plots, we show the best-fit values of $\kappa_\gamma = 1.02^{+0.08}_{-0.07}$ and $\kappa_g = 1.01^{+0.11}_{-0.09}$ along with the 1σ (green) and 2σ (yellow) bands, as was reported on by the ATLAS Collaboration [94].

δf_L and δf_R are the counterterms given by [97]

$$\delta f_L = \frac{m_q e}{2 s_W M_W}\left[1 + \delta Z_e - \frac{\delta s_W}{s_W} + \frac{\delta m_q}{m_q} - \frac{\delta M_W}{M_W} + \frac{1}{2}\delta Z_H + \frac{1}{2}(\delta Z^R_{qq} + \delta Z^{L,\dagger}_{qq})\right],$$
$$\delta f_R = \frac{m_q e}{2 s_W M_W}\left[1 + \delta Z_e - \frac{\delta s_W}{s_W} + \frac{\delta m_q}{m_q} - \frac{\delta M_W}{M_W} + \frac{1}{2}\delta Z_H + \frac{1}{2}(\delta Z^L_{qq} + \delta Z^{R,\dagger}_{qq})\right]. \tag{A6}$$

The renormalization constants δZ are easily calculated:

$$\delta M_Z^2 = \frac{-\alpha s_W^2}{c_W^2 \pi}\left(\frac{-2}{3}A_0(M_S^2) + \frac{4}{3}B_{00}(M_Z^2, M_S^2, M_S^2)\right), \qquad \delta M_W^2 = 0,$$
$$\delta Z_e = \frac{1}{2}\left(-\delta Z_{\gamma\gamma} - \frac{s_W}{c_W}\delta Z_{Z\gamma}\right), \qquad \delta s_W = \frac{c_W^2}{2 s_W}\left(-\frac{\delta M_W^2}{M_W^2} + \frac{\delta M_Z^2}{M_Z^2}\right),$$
$$\delta Z_{\gamma\gamma} = \frac{4\alpha}{3\pi}\frac{\partial}{\partial q^2}B_{00}(q^2, M_S^2, M_S^2)\Big|_{q^2=0}, \qquad \delta Z_H = \frac{3\alpha\lambda_3^2 M_W^2}{\pi s_W^2}\frac{\partial}{\partial q^2}B_0(q^2, M_S^2, M_S^2)\Big|_{q^2=m_H^2},$$
$$\delta Z_{Z\gamma} = \frac{-2\alpha s_W}{c_W M_Z^2 \pi}\left(\frac{-2}{3}A_0(M_S^2) + \frac{4}{3}B_{00}(M_Z^2, M_S^2, M_S^2)\right),$$
$$\delta Z^L_{qq} = \frac{m_q^2 Y_q^2}{16\pi^2}\frac{\partial}{\partial q^2}B_1(q^2, M_\chi^2, M_S^2)\Big|_{q^2=m_q^2}, \qquad \delta m_q = \frac{-1}{32}\frac{m_q Y_q^2}{\pi^2}B_1(m_q^2, M_\chi^2, M_S^2),$$
$$\delta Z^R_{qq} = \frac{Y_q^2}{16\pi^2}\left(B_1(m_q^2, M_\chi^2, M_S^2) + m_q^2\frac{\partial}{\partial q^2}B_1(q^2, M_\chi^2, M_S^2)\Big|_{q^2=m_q^2}\right). \tag{A7}$$

The numerical evaluation of the fermionic decay widths has been done using a customized Python code employing PyCollier [98].[10] The results of our calculations are shown in Fig. 9, where we show κ_u (solid) and κ_c (dashed) as functions of M_χ for $\Delta = 100$ GeV (left), $\Delta = 300$ GeV (middle), and $\Delta = 500$ GeV (right). We can see that unless the couplings Y_q are very large—i.e., $Y_q > 5$ or so—the corrections to κ_q are always small. For large M_χ, all the corrections are decoupling, and κ_q reach their SM values.

[10]PyCollier is a Python wrapper of the Collier library [99].

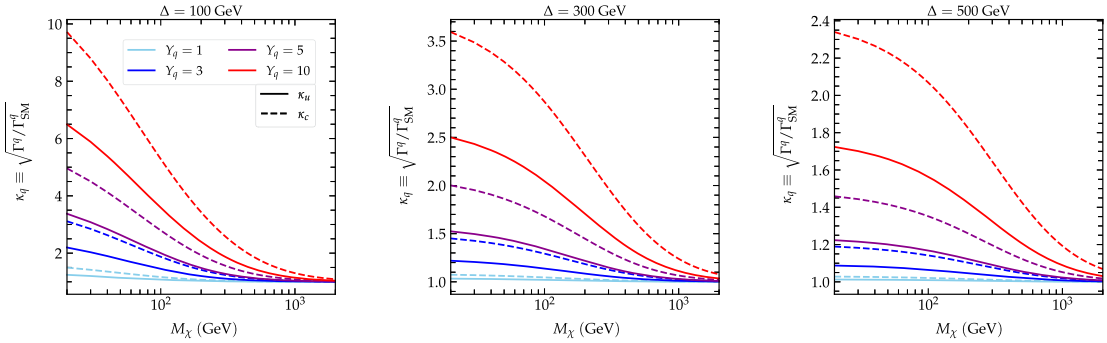

FIG. 9. Dependence of κ_q on the dark matter mass (M_χ) for $\Delta = 100$ GeV (left panel), $\Delta = 300$ GeV (middle panel), and $\Delta = 500$ GeV (right panel). Here, we show the results for κ_c (solid lines) and κ_u (dashed lines). For each panel, the results are shown for $Y_q = 1$ (purple), $Y_q = 3$ (blue), $Y_q = 5$ (purple), and $Y_q = 10$ (red).

APPENDIX B: CONTRIBUTION TO THE ρ PARAMETER

In this section, we demonstrate that our model gives a zero contribution to the ρ parameter (this was mentioned in Sec. II). We explicitly calculate the contribution to the ρ parameter at the one-loop order, where the leading-order Feynman diagrams in this model are shown in Fig. 10. The expression of $\Delta\rho$ is given by

$$\Delta\rho = \left(\frac{\Pi_{ZZ}(0)}{M_Z^2} - \frac{\Pi_{WW}(0)}{M_W^2} - \frac{2s_W}{c_W}\frac{\Pi_{Z\gamma}(0)}{M_Z^2}\right), \quad \text{(B1)}$$

where $\Pi_{VV'}(q^2)$ is the contribution to the 1PI two-point function, and $s_W = \sin^2\theta_W$ is the sine of the Weinberg mixing angle. Since the colored scalar mediator is a singlet under $SU(2)_L$, its contribution to the W-boson self energy is exactly zero. Using FeynArts and FormCalc, we have

$$\Pi_{ZZ}(0) = -\frac{g_1^2 s_W^2}{\pi^2}\left(\frac{1}{6}A_0(M_S^2) - \frac{1}{3}B_{00}(0, M_S^2, M_S^2)\right),$$
$$\Pi_{Z\gamma}(0) = \frac{g_1^2 s_W c_W}{\pi^2}\left(\frac{1}{6}A_0(M_S^2) - \frac{1}{3}B_{00}(0, M_S^2, M_S^2)\right), \quad \text{(B2)}$$

where $A_0(x)$ and $B_{00}(0, x, x)$ are the one- and two-point scalar loop functions, and $g_1 = e/c_W$ is the $U(1)_Y$ gauge coupling. We get

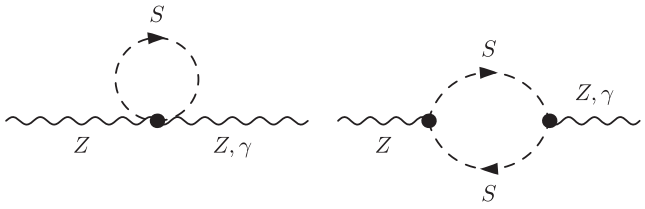

FIG. 10. Examples of Feynman diagrams that contribute to ZZ and $Z\gamma$ self-energies at the one-loop order.

$$\Delta\rho = -\frac{3g_1^2 s_W^2}{\pi^2 M_Z^2}\left(\frac{1}{6}A_0(M_S^2) - \frac{1}{3}B_{00}(0, M_S^2, M_S^2)\right). \quad \text{(B3)}$$

We must note that $\Delta\rho$ given above is free of UV divergences, since the UV divergent part of the two Passarino-Veltman functions is

$$\mathrm{Div}[A_0(m^2)] \equiv m^2\Delta,$$
$$\mathrm{Div}[B_{00}(p^2, m_1^2, m_2^2)] \equiv \left(\frac{m_1^2 + m_2^2}{4} - \frac{p^2}{2}\right)\Delta, \quad \text{(B4)}$$

where $\Delta = 2/\epsilon + \log(4\pi) - \gamma_E$. In our case, the UV-divergent parts of A_0 and B_{00} satisfy $\mathrm{Div}[A_0] = 2 \times \mathrm{Div}[B_{00}]$, which implies that $\mathrm{Div}[\Delta\rho] = 0$.

APPENDIX C: RENORMALIZATION GROUP EQUATIONS AND HIGH-ENERGY BEHAVIOR

In this section, we show the details of the renormalization group equations (RGEs) relevant for the analysis of Sec. VI. The beta function for a parameter X is given by

$$\beta(X) \equiv \mu\frac{dX}{d\mu} \equiv \frac{1}{(4\pi)^2}\beta^{(1)}(X) + \frac{1}{(4\pi)^4}\beta^{(2)}(X) + \cdots, \quad \text{(C1)}$$

where $\beta^{(1)}(X)$ and $\beta^{(2)}$ refer to the beta functions at the one- and two-loop orders, respectively. Higher-order corrections are encoded in the $\cdots$. The calculation of the beta functions was performed using PyR@Te version 3.0 [100]. Below, we give the expression of the beta functions for the new parameters of the model at the one- and two-loop orders. In what follows, $L_t = (Y_u, Y_c, Y_t)^T$.

1. Dark matter couplings

$$\beta^{(1)}(L_t) = +Y_u^\dagger Y_u L_t + 4L_t L_t^\dagger L_t + 2\mathrm{Tr}(L_t^\dagger L_t)L_t$$
$$-\frac{4}{5}g_1^2 L_t - 4g_3^2 L_t,$$

$$\beta^{(2)}(L_t) = -\frac{1}{4}Y_u^\dagger Y_u Y_u^\dagger Y_u L_t - \frac{1}{4}Y_u^\dagger Y_d Y_d^\dagger Y_u L_t - \frac{3}{2}L_t L_t^\dagger Y_u^\dagger Y_u L_t + 5L_t L_t^\dagger L_t L_t^\dagger L_t - \frac{9}{2}\mathrm{Tr}(Y_u^\dagger Y_u)Y_u^\dagger Y_u L_t - 3\mathrm{Tr}(Y_u^\dagger Y_u L_t L_t^\dagger)L_t$$
$$- \frac{9}{2}\mathrm{Tr}(Y_d^\dagger Y_d)Y_u^\dagger Y_u L_t - \frac{3}{2}\mathrm{Tr}(Y_e^\dagger Y_e)Y_u^\dagger Y_u L_t - 12\mathrm{Tr}(L_t^\dagger L_t L_t^\dagger L_t)L_t - 12\mathrm{Tr}(L_t^\dagger L_t)L_t L_t^\dagger L_t - 8\lambda_3 Y_u^\dagger Y_u L_t$$
$$- 128\lambda_2 L_t L_t^\dagger L_t + 128\lambda_2^2 L_t + 4\lambda_3^2 L_t + \frac{49}{120}g_1^2 Y_u^\dagger Y_u L_t + \frac{51}{8}g_2^2 Y_u^\dagger Y_u L_t - \frac{16}{3}g_3^2 Y_u^\dagger Y_u L_t + \frac{268}{15}g_1^2 L_t L_t^\dagger L_t$$
$$+ \frac{124}{3}g_3^2 L_t L_t^\dagger L_t + \frac{4}{3}g_1^2\mathrm{Tr}(L_t^\dagger L_t)L_t + \frac{20}{3}g_3^2\mathrm{Tr}(L_t^\dagger L_t)L_t + \frac{232}{225}g_1^4 L_t - \frac{64}{15}g_1^2 g_3^2 L_t - \frac{181}{9}g_3^4 L_t.$$

2. Quartic couplings

$$\beta^{(1)}(\lambda_1) = +24\lambda_1^2 + 12\lambda_3^2 - \frac{9}{5}g_1^2\lambda_1 - 9g_2^2\lambda_1 + \frac{27}{200}g_1^4 + \frac{9}{20}g_1^2 g_2^2 + \frac{9}{8}g_2^4 + 12\lambda_1\mathrm{Tr}(Y_u^\dagger Y_u) + 12\lambda_1\mathrm{Tr}(Y_d^\dagger Y_d) + 4\lambda_1\mathrm{Tr}(Y_e^\dagger Y_e)$$
$$- 6\mathrm{Tr}(Y_u^\dagger Y_u Y_u^\dagger Y_u) - 6\mathrm{Tr}(Y_d^\dagger Y_d Y_d^\dagger Y_d) - 2\mathrm{Tr}(Y_e^\dagger Y_e Y_e^\dagger Y_e),$$

$$\beta^{(2)}(\lambda_1) = -312\lambda_1^3 - 120\lambda_1\lambda_3^2 - 96\lambda_3^3 + \frac{108}{5}g_1^2\lambda_1^2 + 108g_2^2\lambda_1^2 + \frac{128}{5}g_1^2\lambda_3^2 + 128g_3^2\lambda_3^2 + \frac{2063}{200}g_1^4\lambda + \frac{117}{20}g_1^2 g_2^2\lambda - \frac{73}{8}g_2^4\lambda$$
$$+ \frac{24}{5}g_1^4\lambda_3 - \frac{3747}{2000}g_1^6 - \frac{1789}{400}g_1^4 g_2^2 - \frac{289}{80}g_1^2 g_2^4 + \frac{305}{16}g_2^6 - 144\lambda_1^2\mathrm{Tr}(Y_u^\dagger Y_u) - 144\lambda_1^2\mathrm{Tr}(Y_d^\dagger Y_d) - 48\lambda_1^2\mathrm{Tr}(Y_e^\dagger Y_e)$$
$$- 48\lambda_3^2\mathrm{Tr}(L_t^\dagger L_t) + \frac{17}{2}g_1^2\lambda_1\mathrm{Tr}(Y_u^\dagger Y_u) + \frac{5}{2}g_1^2\lambda_1\mathrm{Tr}(Y_d^\dagger Y_d) + \frac{15}{2}g_1^2\lambda_1\mathrm{Tr}(Y_e^\dagger Y_e) + \frac{45}{2}g_2^2\lambda_1\mathrm{Tr}(Y_u^\dagger Y_u)$$
$$+ \frac{45}{2}g_2^2\lambda_1\mathrm{Tr}(Y_d^\dagger Y_d) + \frac{15}{2}g_2^2\lambda_1\mathrm{Tr}(Y_e^\dagger Y_e) + 80g_3^2\lambda_1\mathrm{Tr}(Y_u^\dagger Y_u) + 80g_3^2\lambda_1\mathrm{Tr}(Y_d^\dagger Y_d) - \frac{171}{100}g_1^4\mathrm{Tr}(Y_u^\dagger Y_u)$$
$$+ \frac{9}{20}g_1^4\mathrm{Tr}(Y_d^\dagger Y_d) - \frac{9}{4}g_1^4\mathrm{Tr}(Y_e^\dagger Y_e) + \frac{63}{10}g_1^2 g_2^2\mathrm{Tr}(Y_u^\dagger Y_u) + \frac{27}{10}g_1^2 g_2^2\mathrm{Tr}(Y_d^\dagger Y_d) + \frac{33}{10}g_1^2 g_2^2\mathrm{Tr}(Y_e^\dagger Y_e) - \frac{9}{4}g_2^4\mathrm{Tr}(Y_u^\dagger Y_u)$$
$$- \frac{9}{4}g_2^4\mathrm{Tr}(Y_d^\dagger Y_d) - \frac{3}{4}g_2^4\mathrm{Tr}(Y_e^\dagger Y_e) - 3\lambda_1\mathrm{Tr}(Y_u^\dagger Y_u Y_u^\dagger Y_u) - 18\lambda_1\mathrm{Tr}(Y_u^\dagger Y_u L_t L_t^\dagger) - 42\lambda_1\mathrm{Tr}(Y_u^\dagger Y_d Y_d^\dagger Y_u)$$
$$- 3\lambda_1\mathrm{Tr}(Y_d^\dagger Y_d Y_d^\dagger Y_d) - \lambda_1\mathrm{Tr}(Y_e^\dagger Y_e Y_e^\dagger Y_e) - \frac{8}{5}g_1^2\mathrm{Tr}(Y_u^\dagger Y_u Y_u^\dagger Y_u) + \frac{4}{5}g_1^2\mathrm{Tr}(Y_d^\dagger Y_d Y_d^\dagger Y_d) - \frac{12}{5}g_1^2\mathrm{Tr}(Y_e^\dagger Y_e Y_e^\dagger Y_e)$$
$$- 32g_3^2\mathrm{Tr}(Y_u^\dagger Y_u Y_u^\dagger Y_u) - 32g_3^2\mathrm{Tr}(Y_d^\dagger Y_d Y_d^\dagger Y_d) + 30\mathrm{Tr}(Y_u^\dagger Y_u Y_u^\dagger Y_u Y_u^\dagger Y_u) + 12\mathrm{Tr}(Y_u^\dagger Y_u Y_u^\dagger Y_u L_t L_t^\dagger)$$
$$- 6\mathrm{Tr}(Y_u^\dagger Y_u Y_u^\dagger Y_d Y_d^\dagger Y_u) - 6\mathrm{Tr}(Y_u^\dagger Y_d Y_d^\dagger Y_d Y_d^\dagger Y_u) + 30\mathrm{Tr}(Y_d^\dagger Y_d Y_d^\dagger Y_d Y_d^\dagger Y_d) + 10\mathrm{Tr}(Y_e^\dagger Y_e Y_e^\dagger Y_e Y_e^\dagger Y_e),$$

$$\beta^{(1)}(\lambda_2) = +112\lambda_2^2 + 2\lambda_3^2 - \frac{16}{5}g_1^2\lambda_2 - 16g_3^2\lambda_2 + \frac{8}{75}g_1^4 + \frac{4}{15}g_1^2 g_3^2 + \frac{13}{24}g_3^4 + 8\lambda_2\mathrm{Tr}(L_t^\dagger L_t) - 2\mathrm{Tr}(L_t^\dagger L_t L_t^\dagger L_t),$$

$$\beta^{(2)}(\lambda_2) = -6144\lambda_2^3 - 80\lambda_2\lambda_3^2 - 16\lambda_3^3 + \frac{2816}{15}g_1^2\lambda_2^2 + \frac{2816}{3}g_3^2\lambda_2^2 + \frac{12}{5}g_1^2\lambda_3^2 + 12g_2^2\lambda_3^2 + \frac{5732}{225}g_1^4\lambda_2 + \frac{704}{45}g_1^2 g_3^2\lambda_2 - \frac{212}{3}g_3^4\lambda_2$$
$$+ \frac{4}{5}g_1^4\lambda_3 - \frac{5416}{3375}g_1^6 - \frac{2554}{675}g_1^4 g_3^2 - \frac{398}{135}g_1^2 g_3^4 + \frac{349}{27}g_3^6 - 448\lambda_2^2\mathrm{Tr}(L_t^\dagger L_t) - 12\lambda_3^2\mathrm{Tr}(Y_u^\dagger Y_u) - 12\lambda_3^2\mathrm{Tr}(Y_d^\dagger Y_d)$$
$$- 4\lambda_3^2\mathrm{Tr}(Y_e^\dagger Y_e) + \frac{16}{3}g_1^2\lambda_2\mathrm{Tr}(L_t^\dagger L_t) + \frac{80}{3}g_3^2\lambda_2\mathrm{Tr}(L_t^\dagger L_t) - \frac{32}{225}g_1^4\mathrm{Tr}(L_t^\dagger L_t) - \frac{16}{45}g_1^2 g_3^2\mathrm{Tr}(L_t^\dagger L_t) - \frac{13}{18}g_3^4\mathrm{Tr}(L_t^\dagger L_t)$$
$$- 12\lambda_2\mathrm{Tr}(Y_u^\dagger Y_u L_t L_t^\dagger) - 16\lambda_2\mathrm{Tr}(L_t^\dagger L_t L_t^\dagger L_t) + 4\mathrm{Tr}(Y_u^\dagger Y_u L_t L_t^\dagger L_t L_t^\dagger) + 24\mathrm{Tr}(L_t^\dagger L_t L_t^\dagger L_t L_t^\dagger L_t),$$

$$\beta^{(1)}(\lambda_3) = +12\lambda_1\lambda_3 + 64\lambda_2\lambda_3 + 8\lambda_3^2 - \frac{5}{2}g_1^2\lambda_3 - \frac{9}{2}g_2^2\lambda_3 - 8g_3^2\lambda_3 + \frac{6}{25}g_1^4 + 6\lambda_3\mathrm{Tr}(Y_u^\dagger Y_u) + 6\lambda_3\mathrm{Tr}(Y_d^\dagger Y_d) + 2\lambda_3\mathrm{Tr}(Y_e^\dagger Y_e)$$
$$+ 4\lambda_3\mathrm{Tr}(L_t^\dagger L_t) - 4\mathrm{Tr}(Y_u^\dagger Y_u L_t L_t^\dagger),$$

$$\begin{aligned}\beta^{(2)}(\lambda_3) = &-144\lambda_1\lambda_3^2 - 768\lambda_2\lambda_3^2 - 60\lambda_1^2\lambda_3 - 1280\lambda_2^2\lambda_3 - 52\lambda_3^3 + \frac{72}{5}g_1^2\lambda_1\lambda_3 + 72g_2^2\lambda_1\lambda_3 + \frac{2048}{15}g_1^2\lambda_2\lambda_3 + \frac{2048}{3}g_3^2\lambda_2\lambda_3 \\ &+ \frac{10}{3}g_1^2\lambda_3^2 + 6g_2^2\lambda_3^2 + \frac{32}{3}g_3^2\lambda_3^2 + \frac{12}{5}g_1^4\lambda + \frac{64}{5}g_1^4\lambda_2 + \frac{57487}{3600}g_1^4\lambda_3 + \frac{9}{8}g_1^2g_2^2\lambda_3 + \frac{32}{9}g_1^2g_3^2\lambda_3 - \frac{145}{16}g_2^4\lambda_3 - 44g_3^4\lambda_3 \\ &- \frac{2603}{750}g_1^6 - \frac{9}{10}g_1^4g_2^2 - \frac{8}{5}g_1^4g_3^2 - 72\lambda_1\lambda_3\mathrm{Tr}(Y_u^\dagger Y_u) - 72\lambda_1\lambda_3\mathrm{Tr}(Y_d^\dagger Y_d) - 24\lambda_1\lambda_3\mathrm{Tr}(Y_e^\dagger Y_e) - 256\lambda_2\lambda_3\mathrm{Tr}(L_t^\dagger L_t) \\ &- 24\lambda_3^2\mathrm{Tr}(Y_u^\dagger Y_u) - 24\lambda_3^2\mathrm{Tr}(Y_d^\dagger Y_d) - 8\lambda_3^2\mathrm{Tr}(Y_e^\dagger Y_e) - 16\lambda_3^2\mathrm{Tr}(L_t^\dagger L_t) + \frac{17}{4}g_1^2\lambda_3\mathrm{Tr}(Y_u^\dagger Y_u) + \frac{5}{4}g_1^2\lambda_3\mathrm{Tr}(Y_d^\dagger Y_d) \\ &+ \frac{15}{4}g_1^2\lambda_3\mathrm{Tr}(Y_e^\dagger Y_e) + \frac{8}{3}g_1^2\lambda_3\mathrm{Tr}(L_t^\dagger L_t) + \frac{45}{4}g_2^2\lambda_3\mathrm{Tr}(Y_u^\dagger Y_u) + \frac{45}{4}g_2^2\lambda_3\mathrm{Tr}(Y_d^\dagger Y_d) + \frac{15}{4}g_2^2\lambda_3\mathrm{Tr}(Y_e^\dagger Y_e) \\ &+ 40g_3^2\lambda_3\mathrm{Tr}(Y_u^\dagger Y_u) + 40g_3^2\lambda_3\mathrm{Tr}(Y_d^\dagger Y_d) + \frac{40}{3}g_3^2\lambda_3\mathrm{Tr}(L_t^\dagger L_t) - \frac{38}{25}g_1^4\mathrm{Tr}(Y_u^\dagger Y_u) + \frac{2}{5}g_1^4\mathrm{Tr}(Y_d^\dagger Y_d) - 2g_1^4\mathrm{Tr}(Y_e^\dagger Y_e) \\ &- \frac{4}{25}g_1^4\mathrm{Tr}(L_t^\dagger L_t) - 16g_3^4\mathrm{Tr}(Y_u^\dagger Y_u) - 16g_3^4\mathrm{Tr}(Y_d^\dagger Y_d) - \frac{27}{2}\lambda_3\mathrm{Tr}(Y_u^\dagger Y_u Y_u^\dagger Y_u) + \lambda_3\mathrm{Tr}(Y_u^\dagger Y_u L_t L_t^\dagger) \\ &- 21\lambda_3\mathrm{Tr}(Y_u^\dagger Y_d Y_d^\dagger Y_u) - \frac{27}{2}\lambda_3\mathrm{Tr}(Y_d^\dagger Y_d Y_d^\dagger Y_d) - \frac{9}{2}\lambda_3\mathrm{Tr}(Y_e^\dagger Y_e Y_e^\dagger Y_e) - 24\lambda_3\mathrm{Tr}(L_t^\dagger L_t L_t^\dagger L_t) - \frac{8}{15}g_1^2\mathrm{Tr}(Y_u^\dagger Y_u L_t L_t^\dagger) \\ &- \frac{32}{3}g_3^2\mathrm{Tr}(Y_u^\dagger Y_u L_t L_t^\dagger) + 14\mathrm{Tr}(Y_u^\dagger Y_u Y_u^\dagger Y_u L_t L_t^\dagger) + 44\mathrm{Tr}(Y_u^\dagger Y_u L_t L_t^\dagger L_t L_t^\dagger) - 2\mathrm{Tr}(Y_u^\dagger Y_d Y_d^\dagger Y_u L_t L_t^\dagger).\end{aligned}$$

[1] S. L. Glashow, J. Iliopoulos, and L. Maiani, Weak interactions with lepton-hadron symmetry, Phys. Rev. D **2**, 1285 (1970).

[2] G. Eilam, J. L. Hewett, and A. Soni, Rare decays of the top quark in the standard and two Higgs doublet models, Phys. Rev. D **44**, 1473 (1991); Phys. Rev. D **59**, 039901(E) (1999).

[3] W.-S. Hou, Tree level $t \to ch^0$ or $h^0 \to t\bar{c}$ decays, Phys. Lett. B **296**, 179 (1992).

[4] D. Atwood, L. Reina, and A. Soni, Phenomenology of two Higgs doublet models with flavor changing neutral currents, Phys. Rev. D **55**, 3156 (1997).

[5] J. L. Lopez, D. V. Nanopoulos, and R. Rangarajan, New supersymmetric contributions to $t \to cV$, Phys. Rev. D **56**, 3100 (1997).

[6] J. M. Yang, B.-L. Young, and X. Zhang, Flavor changing top quark decays in R-parity violating SUSY, Phys. Rev. D **58**, 055001 (1998).

[7] G. Eilam, A. Gemintern, T. Han, J. M. Yang, and X. Zhang, Top quark rare decay $t \to ch$ in R-parity violating SUSY, Phys. Lett. B **510**, 227 (2001).

[8] J. A. Aguilar-Saavedra, Top flavor-changing neutral interactions: Theoretical expectations and experimental detection, Acta Phys. Pol. B **35**, 2695 (2004), https://inspirehep.net/literature/660681.

[9] R. Gaitan, O. G. Miranda, and L. G. Cabral-Rosetti, Rare top and Higgs decays in alternative left-right symmetric models, Phys. Rev. D **72**, 034018 (2005).

[10] M. Frank and I. Turan, $t \to cg$, $c\gamma$, cZ in the left-right supersymmetric model, Phys. Rev. D **72**, 035008 (2005).

[11] S. Bejar, Flavor changing neutral decay effects in models with two Higgs boson doublets: Applications to LHC Physics, Other thesis, Universitat Autonoma de Barcelona, 2006.

[12] K. Agashe, G. Perez, and A. Soni, Collider signals of top quark flavor violation from a warped extra dimension, Phys. Rev. D **75**, 015002 (2007).

[13] J. J. Cao, G. Eilam, M. Frank, K. Hikasa, G. L. Liu, I. Turan, and J. M. Yang, SUSY-induced FCNC top-quark processes at the Large Hadron Collider, Phys. Rev. D **75**, 075021 (2007).

[14] I. Baum, G. Eilam, and S. Bar-Shalom, Scalar flavor changing neutral currents and rare top quark decays in a two Higgs doublet model "for the top quark", Phys. Rev. D **77**, 113008 (2008).

[15] X.-F. Han, L. Wang, and J. M. Yang, Top quark FCNC decays and productions at LHC in littlest Higgs model with T-parity, Phys. Rev. D **80**, 015018 (2009).

[16] K. Agashe and R. Contino, Composite Higgs-mediated FCNC, Phys. Rev. D **80**, 075016 (2009).

[17] T.-J. Gao, T.-F. Feng, and J.-B. Chen, $t \to c\gamma$ and $t \to cg$ in warped extra dimensions, J. High Energy Phys. 02 (2013) 029.

[18] A. Dedes, M. Paraskevas, J. Rosiek, K. Suxho, and K. Tamvakis, Rare top-quark decays to Higgs boson in MSSM, J. High Energy Phys. 11 (2014) 137.

[19] G. Abbas, A. Celis, X.-Q. Li, J. Lu, and A. Pich, Flavour-changing top decays in the aligned two-Higgs-doublet model, J. High Energy Phys. 06 (2015) 005.

[20] F. J. Botella, G. C. Branco, M. Nebot, and M. N. Rebelo, Flavour changing Higgs couplings in a class of two Higgs doublet models, Eur. Phys. J. C **76**, 161 (2016).

[21] U. K. Dey and T. Jha, Rare top decays in minimal and nonminimal universal extra dimension models, Phys. Rev. D **94**, 056011 (2016).

[22] A. Diaz-Furlong, M. Frank, N. Pourtolami, M. Toharia, and R. Xoxocotzi, Flavor-changing decays of the top quark in 5D warped models, Phys. Rev. D **94**, 036001 (2016).

[23] P. Q. Hung, Y.-X. Lin, C. S. Nugroho, and T.-C. Yuan, Top quark rare decays via loop-induced FCNC interactions in extended mirror fermion model, Nucl. Phys. **B927**, 166 (2018).

[24] T. J. Kim, P. Ko, J. Li, J. Park, and P. Wu, Correlation between $R_{D^{(*)}}$ and top quark FCNC decays in leptoquark models, J. High Energy Phys. 07 (2019) 025.

[25] S. Banerjee, M. Chala, and M. Spannowsky, Top quark FCNCs in extended Higgs sectors, Eur. Phys. J. C **78**, 683 (2018).

[26] A. Bolaños, R. Sánchez-Vélez, and G. Tavares-Velasco, Flavor changing neutral current decays $t \to cX$ ($X = \gamma$, g, Z, H) and $t \to c\bar{\ell}\ell$ ($\ell = \mu$, τ) via scalar leptoquarks, Eur. Phys. J. C **79**, 700 (2019).

[27] Y. Liu, B. Yan, and R. Zhang, Loop induced top quark FCNC through top quark and dark matter interactions, Phys. Lett. B **827**, 136964 (2022).

[28] C.-H. Chen and T. Nomura, Scotogenic top-quark FCNC decays, Phys. Rev. D **106**, 095005 (2022).

[29] A. Crivellin, M. Kirk, T. Kitahara, and F. Mescia, Large $t \to cZ$ as a sign of vectorlike quarks in light of the W mass, Phys. Rev. D **106**, L031704 (2022).

[30] C.-H. Chen, C.-W. Chiang, and C.-W. Su, Top-quark FCNC decays, LFVs, lepton $g-2$, and W mass anomaly with inert charged Higgses, J. Phys. G **51**, 085001 (2024).

[31] M. Frank, B. Fuks, S. K. Garg, and P. Poulose, Flavour-changing top quark decays in the alternative left-right model, Phys. Lett. B **850**, 138548 (2024).

[32] G. Aad *et al.* (ATLAS Collaboration), Search for flavour-changing neutral current top-quark decays to qZ in pp collision data collected with the ATLAS detector at $\sqrt{s} = 8$ TeV, Eur. Phys. J. C **76**, 12 (2016).

[33] G. Aad *et al.* (ATLAS Collaboration), Search for flavour-changing neutral current top quark decays $t \to Hq$ in pp collisions at $\sqrt{s} = 8$ TeV with the ATLAS detector, J. High Energy Phys. 12 (**2015**) 061.

[34] M. Aaboud *et al.* (ATLAS Collaboration), Search for top quark decays $t \to qH$, with $H \to \gamma\gamma$, in $\sqrt{s} = 13$ TeV pp collisions using the ATLAS detector, J. High Energy Phys. 10 (2017) 129.

[35] M. Aaboud *et al.* (ATLAS Collaboration), Search for flavour-changing neutral current top-quark decays $t \to qZ$ in proton-proton collisions at $\sqrt{s} = 13$ TeV with the ATLAS detector, J. High Energy Phys. 07 (2018) 176.

[36] M. Aaboud *et al.* (ATLAS Collaboration), Search for flavor-changing neutral currents in top quark decays $t \to Hc$ and $t \to Hu$ in multilepton final states in proton-proton collisions at $\sqrt{s} = 13$ TeV with the ATLAS detector, Phys. Rev. D **98**, 032002 (2018).

[37] M. Aaboud *et al.* (ATLAS Collaboration), Search for top-quark decays $t \to Hq$ with 36 fb^{-1} of pp collision data at $\sqrt{s} = 13$ TeV with the ATLAS detector, J. High Energy Phys. 05 (2019) 123,

[38] G. Aad *et al.* (ATLAS Collaboration), Search for flavour-changing neutral currents in processes with one top quark and a photon using 81 fb^{-1} of pp collisions at $\sqrt{s} = 13$ TeV with the ATLAS experiment, Phys. Lett. B **800**, 135082 (2020).

[39] G. Aad *et al.* (ATLAS Collaboration), Search for flavour-changing neutral-current interactions of a top quark and a gluon in pp collisions at $\sqrt{s} = 13$ TeV with the ATLAS detector, Eur. Phys. J. C **82**, 334 (2022).

[40] G. Aad *et al.* (ATLAS Collaboration), Search for flavour-changing neutral-current couplings between the top quark and the photon with the ATLAS detector at $s = 13$ TeV, Phys. Lett. B **842**, 137379 (2023).

[41] G. Aad *et al.* (ATLAS Collaboration), Search for flavor-changing neutral-current couplings between the top quark and the Z boson with proton-proton collisions at $s = 13$ TeV with the ATLAS detector, Phys. Rev. D **108**, 032019 (2023).

[42] G. Aad *et al.* (ATLAS Collaboration), Search for flavor-changing neutral tqH interactions with $H \to \gamma\gamma$ in pp collisions at $\sqrt{s} = 13$ TeV using the ATLAS detector, J. High Energy Phys. 12 (**2023**) 195.

[43] S. Chatrchyan *et al.* (CMS Collaboration), Search for flavor-changing neutral currents in top-quark decays $t \to Zq$ in pp collisions at $\sqrt{s} = 8$ TeV, Phys. Rev. Lett. **112**, 171802 (2014).

[44] V. Khachatryan *et al.* (CMS Collaboration), Search for top quark decays via Higgs-boson-mediated flavor-changing neutral currents in pp collisions at $\sqrt{s} = 8$ TeV, J. High Energy Phys. 02 (2017) 079.

[45] A. M. Sirunyan *et al.* (CMS Collaboration), Search for associated production of a Z boson with a single top quark and for tZ flavour-changing interactions in pp collisions at $\sqrt{s} = 8$ TeV, J. High Energy Phys. 07 (2017) 003.

[46] A. M. Sirunyan *et al.* (CMS Collaboration), Search for the flavor-changing neutral current interactions of the top quark and the Higgs boson which decays into a pair of b quarks at $\sqrt{s} = 13$ TeV, J. High Energy Phys. 06 (2018) 102.

[47] A. Tumasyan *et al.* (CMS Collaboration), Search for flavor-changing neutral current interactions of the top quark and the Higgs boson decaying to a bottom quark-antiquark pair at $\sqrt{s} = 13$ TeV, J. High Energy Phys. 02 (2022) 169.

[48] S. Chang, R. Edezhath, J. Hutchinson, and M. Luty, Effective WIMPs, Phys. Rev. D **89**, 015011 (2014).

[49] H. An, L.-T. Wang, and H. Zhang, Dark matter with t-channel mediator: A simple step beyond contact interaction, Phys. Rev. D **89**, 115014 (2014).

[50] A. DiFranzo, K. I. Nagao, A. Rajaraman, and T. M. P. Tait, Simplified models for dark matter interacting with quarks, J. High Energy Phys. 11 (2013) 014; 01 (2014) 162(E).

[51] A. Ibarra and S. Wild, Dirac dark matter with a charged mediator: A comprehensive one-loop analysis of the direct detection phenomenology, J. Cosmol. Astropart. Phys. 05 (2015) 047.

[52] M. Garny, A. Ibarra, and S. Vogl, Signatures of Majorana dark matter with t-channel mediators, Int. J. Mod. Phys. D **24**, 1530019 (2015).

[53] P. Ko, A. Natale, M. Park, and H. Yokoya, Simplified DM models with the full SM gauge symmetry: The case of t-channel colored scalar mediators, J. High Energy Phys. 01 (2017) 086.

[54] S. Baek, P. Ko, and P. Wu, Top-philic scalar dark matter with a vector-like fermionic top partner, J. High Energy Phys. 10 (2016) 117.
[55] T. Abe, J. Kawamura, S. Okawa, and Y. Omura, Dark matter physics, flavor physics and LHC constraints in the dark matter model with a bottom partner, J. High Energy Phys. 03 (2017) 058.
[56] S. Baek, P. Ko, and P. Wu, Heavy quark-philic scalar dark matter with a vector-like fermion portal, J. Cosmol. Astropart. Phys. 07 (2018) 008.
[57] K. A. Mohan, D. Sengupta, T. M. P. Tait, B. Yan, and C. P. Yuan, Direct detection and LHC constraints on a t-channel simplified model of Majorana dark matter at one loop, J. High Energy Phys. 05 (**2019**) 115; 05 (2023) 232(E).
[58] C. Arina, B. Fuks, and L. Mantani, A universal framework for t-channel dark matter models, Eur. Phys. J. C **80**, 409 (2020).
[59] C. Arina, B. Fuks, L. Mantani, H. Mies, L. Panizzi, and J. Salko, Closing in on t-channel simplified dark matter models, Phys. Lett. B **813**, 136038 (2021).
[60] M. Becker, E. Copello, J. Harz, K. A. Mohan, and D. Sengupta, Impact of Sommerfeld effect and bound state formation in simplified t-channel dark matter models, J. High Energy Phys. 08 (**2022**) 145,
[61] C. Arina, B. Fuks, J. Heisig, M. Krämer, L. Mantani, and L. Panizzi, Comprehensive exploration of t-channel simplified models of dark matter, Phys. Rev. D **108**, 115007 (2023).
[62] T. Hahn, Generating Feynman diagrams and amplitudes with FeynArts 3, Comput. Phys. Commun. **140**, 418 (2001).
[63] T. Hahn, A *Mathematica* interface for FormCalc-generated code, Comput. Phys. Commun. **178**, 217 (2008).
[64] T. Hahn, Loop calculations with FeynArts, FormCalc, and LoopTools, Acta Phys. Pol. B **30**, 3469 (1999), https://inspirehep.net/literature/508106.
[65] G. Passarino and M. J. G. Veltman, One loop corrections for e^+e^- annihilation into $\mu^+\mu^-$ in the Weinberg model, Nucl. Phys. **B160**, 151 (1979).
[66] J. M. Soares and A. Barroso, Renormalization of the flavor changing neutral currents, Phys. Rev. D **39**, 1973 (1989).
[67] J. Gao, C. S. Li, and H. X. Zhu, Top quark decay at next-to-next-to-leading order in QCD, Phys. Rev. Lett. **110**, 042001 (2013).
[68] K. Griest and D. Seckel, Three exceptions in the calculation of relic abundances, Phys. Rev. D **43**, 3191 (1991).
[69] G. Servant and T. M. P. Tait, Is the lightest Kaluza-Klein particle a viable dark matter candidate?, Nucl. Phys. **B650**, 391 (2003).
[70] K. Kong and K. T. Matchev, Precise calculation of the relic density of Kaluza-Klein dark matter in universal extra dimensions, J. High Energy Phys. 01 (2006) 038.
[71] G. Bélanger, F. Boudjema, A. Goudelis, A. Pukhov, and B. Zaldivar, micrOMEGAs5.0: Freeze-in, Comput. Phys. Commun. **231**, 173 (2018).
[72] F. Ambrogi, C. Arina, M. Backovic, J. Heisig, F. Maltoni, L. Mantani, O. Mattelaer, and G. Mohlabeng, MadDM v.3.0: A comprehensive tool for dark matter studies, Phys. Dark Universe **24**, 100249 (2019).
[73] G. Belanger *et al.*, Leptoquark manoeuvres in the dark: A simultaneous solution of the dark matter problem and the $R_{D^{(*)}}$ anomalies, J. High Energy Phys. 02 (2022) 042,
[74] K. Agashe *et al.* (Top Quark Working Group), Working group report: Top quark, in Snowmass 2013: Snowmass on the Mississippi, arXiv:1311.2028.
[75] G. Aad *et al.* (ATLAS Collaboration), Search for new phenomena in events with an energetic jet and missing transverse momentum in pp collisions at $\sqrt{s} = 13$ TeV with the ATLAS detector, Phys. Rev. D **103**, 112006 (2021).
[76] E. Conte, B. Fuks, and G. Serret, MadAnalysis 5, A user-friendly framework for collider phenomenology, Comput. Phys. Commun. **184**, 222 (2013).
[77] E. Conte, B. Dumont, B. Fuks, and C. Wymant, Designing and recasting LHC analyses with MadAnalysis 5, Eur. Phys. J. C **74**, 3103 (2014).
[78] B. Dumont, B. Fuks, S. Kraml, S. Bein, G. Chalons, E. Conte, S. Kulkarni, D. Sengupta, and C. Wymant, Toward a public analysis database for LHC new physics searches using MadAnalysis 5, Eur. Phys. J. C **75**, 56 (2015).
[79] E. Conte and B. Fuks, Confronting new physics theories to LHC data with MadAnalysis 5, Int. J. Mod. Phys. A **33**, 1830027 (2018).
[80] D. Agin, Implementation of a search for new physics with jets and missing transverse energy (139/fb; 13 TeV, Report No. ATLAS-EXOT-2018-06, 2023, https://doi.org/10.14428/DVN/REPAMM.
[81] J. Alwall, R. Frederix, S. Frixione, V. Hirschi, F. Maltoni, O. Mattelaer, H. S. Shao, T. Stelzer, P. Torrielli, and M. Zaro, The automated computation of tree-level and next-to-leading order differential cross sections, and their matching to parton shower simulations, J. High Energy Phys. 07 (2014) 079.
[82] R. D. Ball *et al.* (NNPDF Collaboration) Parton distributions from high-precision collider data, Eur. Phys. J. C **77**, 663 (2017).
[83] A. Buckley, J. Ferrando, S. Lloyd, K. Nordström, B. Page, M. Rüfenacht, M. Schönherr, and G. Watt, LHAPDF6: Parton density access in the LHC precision era, Eur. Phys. J. C **75**, 132 (2015).
[84] C. Bierlich *et al.*, A comprehensive guide to the physics and usage of PYTHIA 8.3, SciPost Phys. Codebases **2022**, 8 (2022).
[85] M. Cacciari, G. P. Salam, and G. Soyez, The anti-k_t jet clustering algorithm, J. High Energy Phys. 04 (2008) 063.
[86] M. Cacciari, G. P. Salam, and G. Soyez, FastJet user manual, Eur. Phys. J. C **72**, 1896 (2012).
[87] J. Y. Araz, B. Fuks, and G. Polykratis, Simplified fast detector simulation in MadAnalysis 5, Eur. Phys. J. C **81**, 329 (2021).
[88] L. Heinrich, M. Feickert, G. Stark, and K. Cranmer, Pyhf: Pure-Python implementation of HistFactory statistical models, J. Open Source Software **6**, 2823 (2021).
[89] A. Jueid and S. Kanemura (to be published).
[90] A. Arhrib, R. Benbrik, J. El Falaki, and A. Jueid, Radiative corrections to the triple Higgs coupling in the inert Higgs doublet model, J. High Energy Phys. 12 (2015) 007.
[91] S. Kanemura, M. Kikuchi, and K. Sakurai, Testing the dark matter scenario in the inert doublet model by future precision measurements of the Higgs boson couplings, Phys. Rev. D **94**, 115011 (2016).
[92] S. Kanemura, M. Kikuchi, K. Sakurai, and K. Yagyu, Gauge invariant one-loop corrections to Higgs boson couplings in non-minimal Higgs models, Phys. Rev. D **96**, 035014 (2017).

[93] A. Djouadi, The anatomy of electro-weak symmetry breaking: I. The Higgs boson in the Standard Model, Phys. Rep. **457**, 1 (2008).

[94] ATLAS Collaboration, Measurement of the properties of Higgs boson production at$\sqrt{s} = 13$ TeV in the $H \to \gamma\gamma$ channel using 139 fb^{-1} of pp collision data with the ATLAS experiment, J. High Energy Phys. 07 (2023) 088.

[95] K. G. Chetyrkin, Correlator of the quark scalar currents and $\Gamma_{\rm tot}(H \to \text{hadrons})$ at $\mathcal{O}(\alpha_s^3)$ in pQCD, Phys. Lett. B **390**, 309 (1997).

[96] K. G. Chetyrkin and M. Steinhauser, Complete QCD corrections of order $\mathcal{O}(\alpha_s^3)$ to the hadronic Higgs decay, Phys. Lett. B **408**, 320 (1997).

[97] A. Denner, Techniques for calculation of electroweak radiative corrections at the one loop level and results for W physics at LEP-200, Fortschr. Phys. **41**, 307 (1993).

[98] H. Bahl, J. Braathen, M. Gabelmann, and G. Weiglein, anyH3: Precise predictions for the trilinear Higgs coupling in the Standard Model and beyond, Eur. Phys. J. C **83**, 1156 (2023).

[99] A. Denner, S. Dittmaier, and L. Hofer, Collier: A Fortran-based complex one-loop library in extended regularizations, Comput. Phys. Commun. **212**, 220 (2017).

[100] L. Sartore and I. Schienbein, PyR@Te 3, Comput. Phys. Commun. **261**, 107819 (2021).